Spatio-temporal instability of two superposed fluids in a channel with boundary slip

Geetanjali Chattopadhyay[a], K. C. Sahu[b] and R.Usha[a 1]

[a] *Department of Mathematics, Indian Institute of Technology Madras, Chennai 600036, India*

[b] *Department of Chemical Engineering, Indian Institute of Technology Hyderabad, Kandi, Sangareddy - 502285 Telangana, India*

Abstract

Spatio-temporal stability analysis of a viscosity and density stratified two-fluid flow in a channel with hydrophobic walls, which experience a finite tangential velocity slip, is considered for a range of parameters for which Squire's theorem is not valid. The study restricted only to temporal stability analysis of two/three-dimensional infinitesimal disturbances reveals that three-dimensional disturbances are more unstable than the corresponding two-dimensional disturbances. We examine the role of different types of slip boundary conditions at the channel walls on the temporal growth rate. The influence of velocity slip at the upper wall on the nature of instability in the spatio-temporal framework for low density ratio is investigated, and the boundary that demarcates the convective/absolute instabilities are presented for both two and three-dimensional disturbances. In a configuration with a thinner lower layer away from the upper wall with slip, we found that the flow in the entire domain is absolutely unstable, except for two strips at low and high Reynolds numbers. For the parameters considered in the present study, it is found that the absolutely unstable region shrinks with decrease in velocity slip. The absolute growth rate exhibits a non-monotonic behavior with respect to velocity slip. The role of velocity slip in promoting absolute instability in some parameter regimes suggests that by designing the walls of the channel as hydrophobic/rough/porous surfaces,

[1] Author to whom correspondence should be addressed. Email: ushar@iitm.ac.in

which can be modelled as smooth surfaces with tangential velocity slip, it may be possible to achieve early transition to turbulence in two-layer flow systems.

Keywords: Viscosity and density stratified flow, velocity slip, absolute growth rate, two/three-dimensional disturbances, absolute and convective instabilities

1. Introduction

Several researchers have investigated the stability of two-fluid flows in channels and pipes due to their relevance to practical applications, e.g. the transportation of crude oil in pipelines, mixing of liquids using centerline injectors, upstream of static mixers, the removal of highly viscous or viscoplastic material adhering to pipes by using fast-flowing water streams, to name a few (see for instance Refs. Cao et al. (2003), Joseph et al. (1997), Regner et al. (2007)). An extensive review of the the studies of instabilities in miscible and immiscible two-fluid flows can be found in Govindarajan and Sahu (2014). For the interest of present work, the previous studies associated with immiscible systems are only reviewed below.

The pioneering work of Yih (1967) considered the interfacial instability of two immiscible fluids, and demonstrated that instability exists due to an interfacial mode even in the limit of vanishingly small Reynolds numbers. Later, Yiantsios and Higgins (1988) showed that in addition to the unstable interfacial mode, there is an unstable shear mode, which appears at sufficiently large Reynolds numbers. The unstable shear-mode corresponds to the Tollmien-Schlichting mode in a channel flow. Recently, several researchers have conducted linear stability analysis of immiscible fluids, considering the fluids to be Newtonian (Barmak et al., 2016, Kaffel and Riaz, 2015, Mohammadi and Smits, 2017, Tilley et al., 1994, Valluri et al., 2010) and non-Newtonian (Frigaard, 2001, Picchi et al., 2018, Sahu and Matar, 2010, Sahu et al., 2007) and also for gas-liquid systems (Náraigh and Spelt, 2018). In order to understand the mechanism of the interfacial instability, an energy budget analysis was conducted by Boomkamp and Miesen (1996). There are also numerical studies and Direct Numerical

Simulations (DNS) on the dynamics of single/multiphase flow turbulence which are worth mentioning here, due to their capability of capturing all the flow scales down to the smallest (Ahmadi et al., 2016, Náraigh et al., 2014, Rosti and Brandt, 2017, Shankar and Kumaran, 1999, Verma and Kumaran, 2013).

The linear stability analysis of Sahu et al. (2007) was extended by Valluri et al. (2010) and Sahu and Matar (2011) to examine the transition from the convectively unstable to the absolutely unstable regime in case of a channel flow of two immiscible iso-density fluids considering two and three-dimensional disturbances, respectively. In an absolutely unstable flow, disturbances grow locally as well as spread in both upstream and downstream directions, which eventually makes the entire flow regime unstable, whereas in a convectively unstable flow, disturbances amplify as they advect downstream. Valluri et al. (2010) also determined the critical Reynolds number at which transition from convective to absolute instability occurs when one layer is much thinner than the other layer. Sahu and Matar (2011) have pointed out that the three-dimensional disturbances are temporally more unstable than the corresponding two-dimensional disturbances, in a window of parameters for which the flow configuration is absolutely unstable but the growth rates of two-dimensional modes exceed those of three-dimensional modes. Their energy budget analysis provides the information that the interfacial modes are the most dangerous modes.

It is important to note that there are a number of situations in which the velocity of the viscous fluid demonstrates a tangential velocity slip at the walls of the channel. In fact, one can examine two-layer flow in a channel with textured walls at the microscale and/or superhydrophobic surfaces by modeling the walls of the channel as smooth surface with an effective slip at the surface (see for instance Chattopadhyay and Usha (2016), Min and Kim (2005), You and Zheng (2009)). Such a study is also relevant in two-layer flow in a plane channel where one wants to understand the effects of surface roughness of the walls of the channel, as surface roughness is inherent in the process of the manufacture of the system configuration. The advantage of this model is that one can achieve reduction in turbulence drag (Sirovich and Karlsson, 1997) and this provides a

passive means of controlling turbulence effectively in a channel flow.

In fact, wall slip expresses a relation between velocity slip at the wall and the shear stress at the wall with slip-length equal to a local height measured away from the domain and the boundary of the surface where the no-slip condition would be satisfied. The experimental observations of hydrophilic liquid flow in channels with hydrophobic walls at both the micro and nano scales (Ruckenstein and Rajora, 1983, Tretheway and Meinhart, 2002, Watanabe and Udagawa, 2001) and the slip condition

$$u_{slip} = \lambda \frac{\partial u}{\partial y} \tag{1}$$

at the wall proposed by Navier (1823) are consistent with each other. Here, u_{slip} is the velocity of flow at the wall, u is the flow velocity parallel to the wall, λ is the slip length and y is the direction normal to the flow direction. At the microscale, Watanabe et al. (1998), Watanabe and Udagawa (2001) and Watanabe et al. (1999) have observed velocity slip of water flowing over a strongly hydrophobic square channel (15×15 mm) or (6 mm) pipe. The measured velocity profiles are in line with Navier-slip condition at modest Reynolds numbers. The measured slip coefficient varied in the range 5.56×10^{-5} m – 2.5×10^{-4} m. The observed slip length λ varied in the range $0.08 - 0.4$ for water flowing in highly water-repellent pipes and this is reported in experimental investigations (Churaev et al., 1984, Ruckenstein and Rajora, 1983, Tretheway and Meinhart, 2002). In the case of hydrophobic channel, dimensionless slip length was observed to be 0.333 (Tretheway and Meinhart, 2002, Watanabe and Udagawa, 2001). These observed values for slip length λ, yield the bandwidth of dimensionless slip length as $0.0 - 0.2$, when the range of dimensional film thickness is $0.04 - 4\ \mu m$. There are also other experiments reporting the range of slip length as varying from a few nanometers to very high values of more than a thousand micrometers (Mhetar and Archer, 1998, Migler et al., 1993). In the case of a fluid layer of sufficient thickness ranging from tens of micrometers to about 1 mm, the scaled up length ranges upto values of order 10^{-1} (Kalliadasis et al., 2011) and this agrees with the range indicated by Usha and Anjalaiah (2016) and Samanta

et al. (2011). Interestingly, the same order of magnitude for scaled slip length applies when the substrate is composed of a porous material. In this case, the dimensional slip length, $\beta = K_p/\alpha_{BJ}$, the Beavers-Joseph constant takes values from 0.1 to 0.4 (Beavers and Joseph, 1967) and $\sqrt{K_p}$ ranges from very small values to values comparable to 10^{-2} mm (for common porous materials) and K_p is the permeability of the porous medium (Nield and Bejan, 2006). Sadiq *et al.* Sadiq et al. (2010) have considered an example and have taken $\sqrt{K_p}$ as $\sqrt{K_p} = 8.58 \times 10^{-2}$ mm and the characteristic thickness of the fluid layers as 2.4 mm. As constant α_{BJ} varies from its specified values $0.1 - 0.4$, the scaled slip length takes values from 0.0089 to 0.3575. Further, Ellaban et al. (2017) have performed the computations with scaled slip length varying from 0.0 to 0.4. Samanta et al. (2011) have pointed out that the dynamics and stability of a fluid flow over rough/textured/superhydrophobic/grooved (Blake, 1990, Vinogradova, 1995, 1999, Voronov et al., 2008) surfaces can be addressed in terms of the effect of slip at a smooth surface. Blake (1990), Vinogradova (1995, 1999), Voronov et al. (2008) have observed large slip lengths of order of $50\mu m$ in the case of grooved substrates.

In this investigation, slip parameter values considered are based on the experimental observations by Lauga and Cossu (2005) and are the same as in the studies on single or immiscible/miscible two-fluid system in channels with slippery walls (Gersting Jr, 1974, Ghosh et al., 2014a,b, Lauga and Cossu, 2005, Min and Kim, 2005, You and Zheng, 2009). In fact, the range of dimensionless slip parameter values used in the computations are realized for a flow in a hydrophobic channel of height ranging from $0.8\mu m$ ($40\mu m$) to $4\mu m$ ($200\mu m$) and corresponds to a slip length of $20nm$ ($40nm$). It is important to note that the experimental slip length measurements given by Voronov et al. (2008) for different solid surfaces are in accordance with the definition of slip proposed by Blake (1990) and Vinogradova (1995).

Keeping this in view, Chattopadhyay and Usha (2016) have analysed a linear temporal stability analysis of two-dimensional perturbations to the Poiseuille flow of two-immiscible fluids of different viscosities and densities in a hydropho-

bic channel, within the framework of Orr-Sommerfeld system in the presence of an insoluble surfactant at the interface. The effect of slip on the neutral stability boundaries for the interfacial mode has been considered for different thickness ratios of the two-layers with density and/or viscosity differences. The velocity slip at the channel walls shows a promise for control of Yih-Marangoni instability in the corresponding flow system in a rigid channel (Chattopadhyay and Usha, 2016). Further, our preliminary computations clearly indicate that there exists a range of parameters governing the flow system for which the temporal linear stability of the flow configuration in a channel with different combinations of velocity slip at the walls are dominated by three-dimensional disturbances. Thus, it can be expected that the linear spatio-temporal growth of disturbances may be different from those observed by temporal linear stability analyses (Chomaz, 2005, Duprat et al., 2007, Huerre and Monkewitz, 1990, Sahu et al., 2007) in spatially evolving configurations. Thus, the main objective of the present work is to conduct a spatio-temporal analysis of three-dimensional disturbances in a flow of two immiscible fluids in a channel with finite velocity slip at its walls.

At this stage, it is worth recalling the remarks by Yiantsios and Higgins (1988) concerning "Squire's theorem" (Barmak et al., 2017, Drazin and Reid, 2004, Squire, 1933) and Squire's transformation for plane Poiseuille flow of two superposed viscosity and/or density stratified fluids configuration in a rigid channel. Through their analysis on the three-dimensional disturbances, they demonstrated that a Squire's transformation can exist for all flow parameters, but a Squire's theorem can only exist provided the Reynolds number has a destabilizing role. This indicates that there is a necessity to perform three-dimensional stability analysis to assess if two-dimensional disturbances are the most dangerous modes. Keeping in view the observation by Yiantsios and Higgins (1988), the remarks by Sahu and Matar (2011) on the need for performing a linear stability analysis of three-dimensional perturbations to the base state in a pressure-driven two-layer rigid channel flow and the comments by Valluri et al. (2010), the present study, considers the linear spatio-temporal stability analysis of three-dimensional disturbances in a pressure-driven two-layer flow of

fluids with viscosity and/or density contrasts in a hydrophobic channel, whose walls are modelled by a smooth surface with an effective slip at the walls of the channel.

The rest of the paper is organized as follows: the mathematical formulation is presented for viscosity and density stratified two-fluid flow in a slippery channel in §2 and the details of the base state are given in §2.1. A linear temporal stability analysis is discussed in §2.2 for infinitesimal two/three-dimensional disturbances and the temporal growth rates for different types of velocity slip at the channel walls are obtained. In §3, a spatio-temporal stability analysis is presented and boundaries delineating the regions of absolute and convective instabilities in some parameter regimes governing the flow system are presented. The role of slip on absolute growth rate and how this is affected by the inertial effects, viscosity stratification and thickness ratio are assessed. In §4, the highlights of the present study are discussed and §5 presents the concluding remarks.

2. Mathematical formulation

The spatio-temporal linear stability analysis of a fully-developed flow of two immiscible, incompressible viscous fluids of viscosity μ_i and density ρ_i $(i = 1, 2)$ in a channel with hydrophobic walls located at $y = 0$ and $y = H$ $(= d_1 + d_2)$ and modelled by a smooth surface with slip (Min and Kim, 2005) is considered (Fig. 1). Here, the subscripts $i = 1, 2$ represent the properties associated with the top layer (1) and the bottom layer (2), respectively. The flow is due to an imposed uniform pressure gradient, K. Layer '1' is of thickness d_1 with fluid of viscosity μ_1 and density ρ_1, whereas layer '2' is of thickness d_2 with fluid of viscosity μ_2 and density ρ_2. The unperturbed interface is located at $y = d_2$. With respect to a Cartesian (x, y, z) coordinate system, u_i, v_i and w_i denote the velocity components in layer 'i' along the x, y and z directions, respectively. Let p_i denote the pressure and t represents time. The interface separating layer '1' and '2' is located at $y = \eta(x, z, t)$.

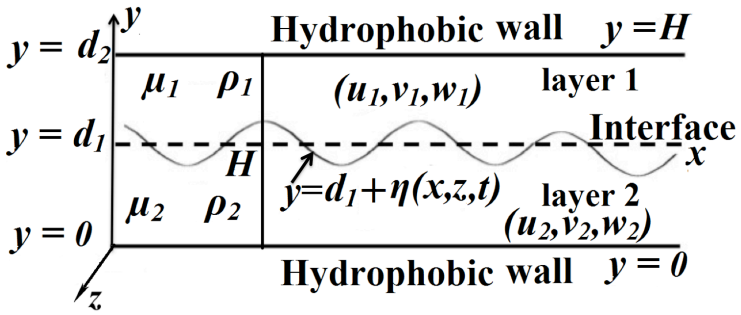

Figure 1: Schematic diagram of three-dimensional flow system considered: two-layer Poiseuille flow in a channel with hydrophobic walls located at $y = 0$ and $y = H(= d_1 + d_2)$. The walls are modelled as smooth surfaces with velocity slip at the walls. The top and bottom layers are represented by layer 1 and layer 2, respectively, d_1 and d_2 are the thicknesses of layer 1 and layer 2, respectively. λ_1 and λ_2 are the slip-lengths at the upper and lower walls, respectively. The density (ρ), viscosity (μ) and velocity field (u, v, w) in layer 1 and 2 are represented by subscripts 1 and 2, respectively.

The height H of the channel is chosen as the length scale, $U_m = Q/H$ as the velocity scale, where Q denotes the total flow rate per unit length in the transverse direction and $\mu_1 U_m/H$ as the pressure scale. Note that, K is the dimensional pressure gradient such that $K = \dfrac{dp_1}{dx} = \dfrac{dp_2}{dx}$. As p_1 and p_2 are made dimensionless with the scale $\dfrac{\mu_1 U_m}{H}$, we have

$$\frac{dp_1^*}{dx^*} = \frac{\frac{dp_1}{dx}}{\frac{\mu_1 U_m}{H^2}}, \quad \frac{dp_2^*}{dx^*} = \frac{\frac{dp_2}{dx}}{\frac{\mu_1 U_m}{H^2}}.$$

Thus,

$$K^* = \frac{dp_1^*}{dx^*} = \frac{dp_2^*}{dx^*} = \frac{KH^2}{\mu_1 U_m}.$$

Note that the quantities presented in the following are dimensionless, and the subscripts t, x, y and z represent the partial derivatives with respect to t, x, y and z, respectively. The dimensionless thickness of the lower layer is $h_l = \dfrac{d_2}{H}$ and the dimensionless pressure gradient is $K^* = \dfrac{KH^2}{\mu_1 U_m}$. The governing equations and boundary conditions are given in terms of the velocity components and the

pressures in the two-layers below. In layer '1' ($h_l \leq y \leq 1$),

$$u_{1x} + v_{1y} + w_{1z} = 0, \tag{2}$$

$$Re[u_{1t} + u_1 u_{1x} + v_1 u_{1y} + w_1 u_{1z}] = -p_{1x} + (u_{1xx} + u_{1yy} + u_{1zz}), \tag{3}$$

$$Re[v_{1t} + u_1 v_{1x} + v_1 v_{1y} + w_1 v_{1z}] = -p_{1y} + (v_{1xx} + v_{1yy} + v_{1zz}) - G_1, \tag{4}$$

$$Re[w_{1t} + u_1 w_{1x} + v_1 w_{1y} + w_1 w_{1z}] = -p_{1z} + (w_{1xx} + w_{1yy} + w_{1zz}), \tag{5}$$

and in layer '2' ($0 \leq y \leq h_l$),

$$u_{2x} + v_{2y} + w_{2z} = 0, \tag{6}$$

$$\frac{r}{m} Re[u_{2t} + u_2 u_{2x} + v_2 u_{2y} + w_2 u_{2z}] = -\frac{1}{m} p_{2x} + (u_{2xx} + u_{2yy} + u_{2zz}), \tag{7}$$

$$\frac{r}{m} Re[v_{2t} + u_2 v_{2x} + v_2 v_{2y} + w_2 v_{2z}] = -\frac{1}{m} p_{2y} + (v_{2xx} + v_{2yy} + v_{2zz}) - \frac{r}{m} G_1, \tag{8}$$

$$\frac{r}{m} Re[w_{2t} + u_2 w_{2x} + v_2 w_{2y} + w_2 w_{2z}] = -\frac{1}{m} p_{2z} + (w_{2xx} + w_{2yy} + w_{2zz}). \tag{9}$$

The boundary conditions at the upper slippery wall ($y = 1$) are

$$u_1 = -\beta_1 u_{1y}, v_1 = 0, w_1 = 0, \tag{10}$$

and at the lower slippery wall ($y = 0$), they are given by

$$u_2 = \beta_2 u_{2y}, v_2 = 0, w_2 = 0, \tag{11}$$

where β_1 and β_2 are dimensionless slip parameters. As mentioned earlier, the magnitude of the dimensionless slip velocity, u_1 or u_2 is proportional to the magnitude of the dimensionless shear rate experienced by the fluid at the wall.

The dimensionless boundary conditions at the interface separating layer '1' and '2' (i.e at $y = h_l + \eta(x, z, t)$) are given below. The continuity of velocity components are

$$u_1 = u_2, v_1 = v_2, w_1 = w_2, \tag{12}$$

and the kinematic boundary condition at $y = h_l + \eta(x, z, t)$ is given by

$$\eta_t = v_1 - u_1 \eta_x - w_1 \eta_z. \tag{13}$$

The balance of shear and normal stresses at $y = h_l + \eta(x, z, t)$ are

$$m[2\eta_x(v_{2y} - u_{2x}) + (u_{2y} + v_{2x})(1 - \eta_x^2) - \eta_z(u_{2z} + w_{2x}) - \eta_x\eta_z(v_{2z} + w_{2y})]$$
$$- [2\eta_x(v_{1y} - u_{1x}) + (u_{1y} + v_{1x})(1 - \eta_x^2) - \eta_z(u_{1z} + w_{1x}) - \eta_x\eta_z(v_{1z} + w_{1y})] = 0, \tag{14}$$

$$m[2\eta_z(v_{2y} - w_{2z}) + (w_{2y} + v_{2z})(1 - \eta_z^2) - \eta_x(u_{2z} + w_{2x}) - \eta_x\eta_z(v_{2x} + u_{2y})]$$
$$- [2\eta_z(v_{1y} - w_{1z}) + (w_{1y} + v_{1z})(1 - \eta_z^2) - \eta_x(u_{1z} + w_{1x}) - \eta_x\eta_z(v_{1x} + u_{1y})] = 0, \tag{15}$$

$$(p_2 - p_1)(1 + \eta_x^2 + \eta_z^2) - 2m[\eta_x^2 u_{2x} - (u_{2y} + v_{2x})\eta_x + v_{2y} + \eta_z^2 w_{2z}$$
$$+ \eta_x\eta_z(u_{2z} + w_{2x}) - \eta_z(v_{2z} + w_{2y})] + 2[\eta_x^2 u_{1x} - (u_{1y} + v_{1x})\eta_x + v_{1y} + \eta_z^2 w_{1z}$$
$$+ \eta_x\eta_z(u_{1z} + w_{1x}) - \eta_z(v_{1z} + w_{1y})] = -\frac{\Gamma_{ic}(\eta_{xx} + \eta_{zz})}{(1 + \eta_x^2 + \eta_z^2)^{\frac{1}{2}}}. \tag{16}$$

Here $m = \mu_2/\mu_1$ and $r = \rho_2/\rho_1$ are the viscosity and density ratios, respectively. The various dimensionless numbers are the Reynolds number, Re $(\equiv \rho_1 H U_m/\mu_1)$, Γ_{ic} $(\equiv \sigma_0/\mu_1 U_m)$, an inverse capillary number and G_1 $\left(\equiv \rho_1 g H^2/\mu_1 U_m\right)$ in which σ_0 denotes the interfacial surface tension and g is the gravitational acceleration. In this study, the focus is on the flow configuration that hosts a high viscous fluid in the lower layer away from the upper wall with velocity slip and with interface location closer to the centerline of the channel.

2.1. Base state

The base state $(U_{iB}, P_{iB},\, i = 1, 2)$ corresponds to a steady, uniform, parallel flow in a slippery channel with a flat interface separating the two-layers. The dimensionless base velocity is given by

$$U_{1B} = \frac{1}{2}K\Big[(y^2 - 1 - 2\beta_1) - \Big\{\frac{m(1 + 2\beta_1) - h_l^2(m - 1)}{m(1 + \beta_1 - h_l) + h_l + \beta_2}\Big\}(y - 1 - \beta_1)\Big], \tag{17}$$

$$U_{2B} = \frac{1}{2m}K\Big[y^2 - \Big\{\frac{m(1 + 2\beta_1) - h_l^2(m - 1)}{m(1 + \beta_1 - h_l) + h_l + \beta_2}\Big\}(y + \beta_2)\Big]. \tag{18}$$

Note that, K in Eqs. (17) and (18) is dimensionless ($*$ notation is suppressed).

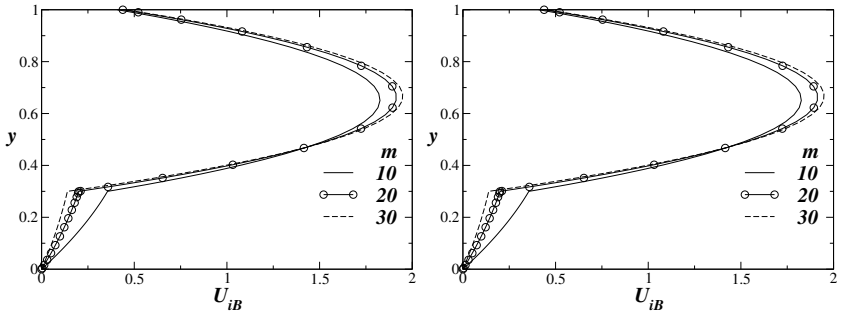

Figure 2: Base state streamwise velocity profiles with no-slip boundary at the lower wall. (a) Effect of velocity slip at the top wall for $m = 20$. (b) Effect of viscosity ratio, m for $\beta_1 = 0.05$. The other parameters are $r = 0.5$, $h_l = 0.3$, $\beta_2 = 0$.

The reduced dimensionless pressure P_{iB} in fluid layer i is obtained in terms of the corresponding dimensional pressure p_i in the i^{th} layer as

$$P_{1B} = \frac{H}{\mu_1 U_m} \left[p_1 + \rho_1 g(y - h_l) \right], \tag{19}$$

$$P_{2B} = \frac{H}{\mu_1 U_m} \left[p_2 + \rho_2 g(y - h_l) \right]. \tag{20}$$

The pressure gradient P is computed using

$$\int_0^{h_l} U_{2B} dy + \int_{h_l}^1 U_{1B} dy = 1. \tag{21}$$

which corresponds to the condition of constant volumetric flow rate. Fig. 2(a) presents the typical base state streamwise velocity (U_{iB}, $i = 1, 2$) profiles when the dimensionless unperturbed interface is at $h_l = 0.3$ for a configuration with lower fluid layer adjacent to a wall without velocity slip ($\beta_2 = 0$) and the upper fluid near the wall with slip ($\beta_1 \neq 0$) or without slip ($\beta_1 = 0$). The channel hosts a high viscous ($m = 20$), low density fluid ($r = 0.5$) in layer '2'. Fig. 2(a) reveals that an increase in slip parameter β_1 increases the velocity at the wall but decreases the velocity inside the upper layer adjacent to the slippery wall. In layer '2' (lower layer), a reverse trend is observed as β_1 increases; however, the differences in velocity are negligibly small. Further, the base velocity for

any velocity slip at the wall is significantly small in the lower layer as compared to that in the upper layer adjacent to slippery wall. The base state profile for different locations of the interface for different values of the slip parameters have also been obtained for different $h_l \in (0.1, 0.8)$ (but not shown). The trend is similar to that in Fig. 2(a) in the sense that the velocity at the centerline for no-slip case (at both the walls) is maximum for any combination of slip/no-slip at the walls. It is remarked that the study does not investigate stability in flow systems with very thin liquid layers (as in Valluri et al. (2010)). Fig. 2(b) shows the effects of viscosity contrast on base state velocity profiles for $\beta_2 = 0$ and $\beta_1 = 0.05$, with the other parameters the same as those in Fig. 2(a). While slip at the upper wall enhances the base velocity in the upper layer as the viscosity contrast (m) increases, the reverse scenario is observed in the lower layer. Further, maximum velocity occurs in the upper layer when the lower layer is thinner and hosting a high viscous fluid.

2.2. Linear stability analysis

A linear temporal stability analysis of the primary flow given by Eqs. (17)−(20) to infinitesimal three-dimensional perturbations is performed using a normal mode analysis by taking

$$(u_i, v_i, w_i, p_i, \zeta_i, \eta) = (U_{iB}(y), 0, 0, P_{iB}, 0, h_l) + \left(\tilde{u}_i(x,y,z,t), \tilde{v}_i(x,y,z,t), \tilde{w}_i(x,y,z,t), \tilde{p}_i(x,y,z,t), \tilde{\zeta}_i(x,y,z,t), \tilde{\eta}(x,z,t)\right), i = 1, 2. \tag{22}$$

Here, the variables with tilde on top denote the perturbed quantities. Note that, $\zeta_i = \partial u_i/\partial z - \partial w_i/\partial x, \quad i = 1, 2$ denote the normal component of the vorticity vector in the two layers and $\tilde{\zeta}_i$ are the normal components of vorticity perturbations in the two layers. Introducing Eq. (22) into Eqs. (2)−(16) and linearising with respect to the perturbation yields the linearised governing equations and boundary conditions for the perturbed quantities. In these, we

replace the perturbed variables by their normal mode expressions given by

$$(\tilde{u}_i, \tilde{v}_i, \tilde{w}_i, \tilde{p}_i, \tilde{\zeta}_i, \tilde{\eta}) = (\hat{u}_i(y), \hat{v}_i(y), \hat{w}_i(y), \hat{p}_i(y), \hat{\zeta}_i(y), h) e^{i(\alpha x + \beta z - \Omega t)}, \quad i = 1, 2, \tag{23}$$

where α and β are the wave numbers in the streamwise (x-direction) and spanwise (z-direction) directions, $\Omega (= \alpha c)$ is the complex pulsation or disturbance frequency and $\hat{\zeta}_i \equiv \partial \hat{u}_i / \partial z - \partial \hat{w}_i / \partial x, \quad i = 1, 2$. Here, c is the perturbation phase speed. This yields the modified Orr-Sommerfeld-Squire system for the two-layers. In layer '1' ($h_l \leq y \leq 1$),

$$i\alpha Re \left[\left\{ D^2 - (\alpha^2 + \beta^2) \right\} (U_{1B} - c) - D^2 U_{1B} \right] v_1 = \left[D^2 - (\alpha^2 + \beta^2) \right]^2 v_1, \tag{24}$$

$$iRe \left[\alpha \zeta_1 (U_{1B} - c) + \beta D U_{1B} v_1 \right] = D^2 \zeta_1 - (\alpha^2 + \beta^2) \zeta_1, \tag{25}$$

and in layer '2' ($0 \leq y \leq h_l$),

$$i\alpha \frac{r}{m} Re \left[\left\{ D^2 - (\alpha^2 + \beta^2) \right\} (U_{2B} - c) - D^2 U_{2B} \right] v_2 = \left[D^2 - (\alpha^2 + \beta^2) \right]^2 v_2, \tag{26}$$

$$i \frac{r}{m} Re \left[\alpha \zeta_2 (U_{2B} - c) + \beta D U_{2B} v_2 \right] = D^2 \zeta_2 - (\alpha^2 + \beta^2) \zeta_2. \tag{27}$$

Note that, the hat decoration in the amplitude of perturbed variables $\hat{v}_i$, $\hat{\zeta}_i$ are suppressed in Eqs. (24)$-$(27), and also in the boundary conditions that follow below. The linearized boundary conditions of velocity slip at the walls of the channel, continuity of velocity, kinematic boundary condition, balance of shear and normal stresses at the interface, are given by

$$Dv_1 = -\beta_1 D^2 v_1, \quad v_1 = 0 \quad \text{at} \quad y = 1, \tag{28}$$

$$Dv_2 = \beta_2 D^2 v_2, \quad v_2 = 0 \quad \text{at} \quad y = 0. \tag{29}$$

At $y = h_l$,

$$Dv_1 - i\alpha h D U_{1B} = Dv_2 - i\alpha h D U_{2B}\,, \tag{30}$$

$$\zeta_1 + i\beta h D U_{1B} = \zeta_2 + i\beta h D U_{2B}\,, \tag{31}$$

$$v_1 = v_2, \tag{32}$$

$$h = \frac{v_1}{i\alpha(U_{1B} - c)} = \frac{v_2}{i\alpha(U_{2B} - c)}, \tag{33}$$

$$m\left[D^2 + (\alpha^2 + \beta^2)\right] v_2 - \frac{(mD^2U_{2B} - D^2U_{1B})}{(U_{1B} - c)} v_1 = \left[D^2 + (\alpha^2 + \beta^2)\right] v_1, \tag{34}$$

$$mD\zeta_2 + \frac{\beta}{\alpha}\frac{(mD^2U_{2B} - D^2U_{1B})}{(U_{1B} - c)} v_1 = D\zeta_1. \tag{35}$$

$$\begin{aligned} i\alpha Re\Big[r\Big\{Dv_2(c - U_{2B}) + DU_{2B}v_2\Big\} - \Big\{Dv_1(c - U_{1B}) + DU_{1B}v_1\Big\}\Big] \\ +m\Big[D^3v_2 - 3(\alpha^2 + \beta^2)Dv_2\Big] - \Big[D^3v_1 + 3(\alpha^2 + \beta^2)Dv_1\Big] \\ = (\alpha^2 + \beta^2)\left\{\Gamma_{ic}(\alpha^2 + \beta^2) + G\right\}\frac{(Dv_1 - Dv_2)}{i\alpha(DU_{1B} - DU_{2B})}, \end{aligned} \tag{36}$$

where $G = (\rho_2 - \rho_1)\, gH^2/\mu_1 U_m$. The mathematical formulation incorporates the gravity effects through the gravity parameter G and this is done in order to generalise the analysis for any flow configuration. Further note that, gravity is accounted for in the stability analysis, but the work focuses on horizontal flows (see Appendix A). The above system of eqs. (24)−(27) and the boundary conditions (28)−(36) dictate the linear temporal stability characteristics of three-dimensional infinitesimal disturbances to the base flow in a two-layer plane Poiseuille flow in a slippery channel. In the absence of slip at the walls, they reduce to the systems in Sahu and Matar (2011), Schmid and Henningson (2012) for Newtonian fluids in a two-layer channel flow.

The above eigenvalue problem (Eqs. (24)−(36)) is discretized using Chebyshev spectral collocation method (Canuto et al., 2012) and numerically solved using LAPACK (a public domain software). We ensure grid independence of our computations by mesh refinement using different orders 'N' of Chebyshev polynomials. The results are not influenced by increasing N, beyond $N = 51$ and so the present results are generated by taking $N = 81$. We have compared

our results with Yiantsios and Higgins (1988) for two-dimensional disturbances ($\beta = 0$) (neutral stability boundaries for two different values of Reynolds numbers; see Fig. 7), with Sahu and Matar (2011) for two ($\beta = 0$) and three-dimensional disturbances ($\beta \neq 0$) (temporal growth rates; see Fig. 3) and with Valluri et al. (2010) (the Reynolds number at which the transition from convective to absolute instability occurs in rigid channel, see Table 2; absolute growth rate; see Fig 14) for two-dimensional disturbance ($\beta = 0$) and we have observed a good agreement. Further, the results on neutral boundaries matched with Chattopadhyay and Usha (2016) for two-fluid flow in a slippery channel in the absence of an insoluble surfactant at the interface (see Fig. 7). This has given us a confidence in the generated results using the developed code. Hence the numerical simulations have been carried out to understand the stability characteristics with respect to two and three-dimensional disturbances. The parameter values are in the range of values for two-fluid systems such as air-water, which are considered in the experimental and theoretical investigations. The results are presented in the following section.

3. Results and discussion

3.1. Results for linear temporal stability analysis

The wave number α and the disturbance frequency Ω obey a dispersion relation (D),

$$D(\alpha, \beta, \Omega, m, r, Re, G, \Gamma_{ic}, \beta_1, \beta_2) = 0. \tag{37}$$

The temporal growth rate, c_i (imaginary part of c) is obtained for the perturbation with a wave number $k_\omega\,(= \sqrt{\alpha^2 + \beta^2};\ \Omega = k_\omega c = \Omega_r + i\Omega_i)$. A positive value of $c_i(= \dfrac{\Omega_i}{k_\omega})$ corresponds to growth of the perturbation amplitude (in time), and a negative value of c_i indicates that the disturbance is damped. The flow parameters for which $c_i = 0$ correspond to neutral stability for the perturbation with wave number, k. If all the perturbations are suppressed or damped, the flow is stable; otherwise it is unstable.

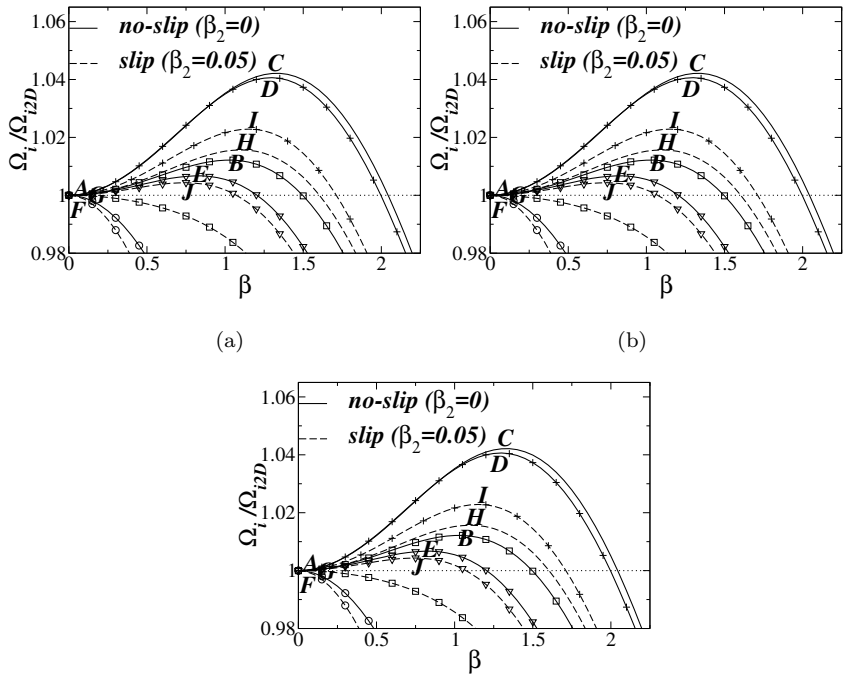

Figure 3: (a) The effect of stronger slip at the lower wall on the normalized growth rate Ω_i/Ω_{i2D} as a function of spanwise wave number β for different streamwise wave number α. Results for different α values are indicated by different symbols: $\alpha = 0.25$ (circle); $\alpha = 0.5$ (square); $\alpha = 0.75$ (no symbol); $\alpha = 1.0$ (plus); $\alpha = 1.5$ (downward triangle), (b) $\alpha = 0.005$ (no symbol), $\alpha = 0.1$ (plus), $\alpha = 0.2$ (circle), (c) $\alpha = 1.6$ (no symbol), $\alpha = 1.8$ (plus), $\alpha = 2$ (circle). The rest of the parameters are $\beta_1 = 0$, $Re = 500$, $h_l = 0.3$, $m = 30$, $r = 1.2$, $\Gamma_{ic} = 0.01$ and $G = 10$.

The variations in normalized growth rate Ω_i/Ω_{i2D} versus β (wave number in the spanwise direction) are presented in Fig. 3(a) for different values of streamwise wave number (α), where Ω_{i2D} corresponds to the linear temporal growth rate for the two-dimensional disturbances ($\beta = 0$). The results with stronger slip at the lower wall (dashed curves; $\beta_1 = 0, \beta_2 = 0.05$) are compared with the no-slip case (solid curves, $\beta_1 = \beta_2 = 0$; Sahu and Matar (2011)), when $Re = 500$, $\Gamma_{ic} = 0.01$ and $G = 10$. The lower thinner layer ($h_l = 0.3$) hosts high viscous ($m = 30$) and high density ($r = 1.2$) fluid. The dispersion curves reveal

that for a fixed β, the normalized growth rates in a slippery channel are less than those in a channel with rigid walls, for each value of α. In a slippery channel, there is an increase in the maximum normalized growth rate as α increases. This happens up to $\alpha = 1$ in a slippery channel ($\alpha = 0.75$ in the rigid case) and then decreases with increase in α. The range of β for which $\Omega_i > \Omega_{i2D}$ increases with decrease in α up to $\alpha = 1$, but with further decrease in α, the range of β decreases (see for $\alpha = 0.75$, dashed curve with no symbol). We infer from Fig. 3(a) that, in the presence of stronger slip at the lower wall, the temporal linear instability in a system with high viscous and high density fluid in a thinner layer adjacent to the lower wall with slip is dominated by three-dimensional perturbations for some values of streamwise wave numbers (α) in a bandwidth of values of spanwise wave numbers (β). Note that for $\alpha < 0.5$ (curves with circles), the instability due to two-dimensional disturbances is dominant (since $\Omega_i/\Omega_{i2D} < 1$). However, while the above is true for the stronger slip at the lower wall case for $\alpha = 0.5$ (dashed curves with squares), it is not so for the channel configuration with no-slip at the walls (solid curves with squares). It is of interest to see the trend in the long and short wave number regimes and the results are presented in Fig. 3(b) and Fig. 3(c), respectively. In the long as well as short wave regimes, the two-dimensional disturbances are dominant. The results indicate that there is a window (α_l, α_u) of wave numbers where the three-dimensional disturbances are dominant (both for no-slip and slip cases) and outside this bandwidth, the two-dimensional disturbances are dominant for the flow system with stronger-slip at the lower wall. For all α, the slip has tendency to stabilize the flow system with no-slip at the wall, by decreasing the normalised growth rate. The other slip cases (symmetric slip at the walls: $\beta_1 = 0.05, \beta_2 = 0.05$, strong slip at the upper wall: $\beta_1 = 0.05, \beta_2 = 0$) also exhibit (fig not shown) a similar behaviour in the long and short wave regimes, namely, two-dimensional disturbances dominate the long and short wave regimes whereas in a moderate wave number window (which varies for different slip conditions), the three-dimensional perturbations are dominant with slip playing a stabilising role by decreasing the growth rate for all wave numbers.

Table 1: Energy Budget for points labelled $A, B, C, D, E, F, G, H, I, J$ in Fig. 3(a).

Points	REY_2	REY_1	DIS_2	DIS_1	TAN_x	TAN_z	TEN	HYD
A	0	0.0043	-0.0066	-0.0298	1.0322	0	0	0
B	0	0.0198	-0.0037	-0.0326	1.0253	-0.0088	0	0
C	0	0.0295	-0.0064	-0.0319	1.0205	-0.0148	0	0
D	0	0.0372	-0.0094	-0.0307	1.0216	-0.0188	0	0
E	0	0.0477	-0.0151	0.0279	1.0153	-0.0201	0	0.0001
F	0	0.0054	-0.0060	-0.0285	1.0290	0	0	0
G	0	0.0137	-0.0084	-0.0275	1.0222	0	0	0
H	0	0.0340	-0.0052	-0.0318	1.0181	-0.0152	0	0
I	0.0001	0.0436	-0.0074	-0.0311	1.0150	-0.0203	0	0
J	0.0001	0.0518	-0.0132	-0.0265	1.0025	-0.0148	0	0.0001

The physical mechanism that is responsible for this instability can be explained through energy budget analysis (Hinch, 1984) (Appendix B). As in the no-slip case (Sahu and Matar, 2011), the largest contribution to the rate of change of disturbance kinetic energy, KIN comes from the work done by the disturbance velocity and disturbance stresses in the streamwise direction, TAN_x, in the case of strong slip at the lower wall and no-slip at the upper wall of the channel. In this case, note that the lower layer hosts a high viscous fluid having larger density. As, a consequence, the unstable mode is the interface mode which arises due to stratification. The Reynolds stress REY_1 in the upper fluid is also positive and contributes to KIN, but it is comparatively smaller than TAN_x (Table 1). Further, REY_1 increases with increase in α; however, REY_2 has negligible contribution to KIN. The contribution from viscous dissipation energy terms DIS_1 and DIS_2 are negative and they act as a restoring force; in view of this, they have a stabilizing role. The total dissipative energy decreases with increasing α and the total positive contribution from REY_1 and

TAN_x is non-monotonic; it increases with increase in α, reaching a maximum at $\alpha = 1$ and with further increase in α, it decreases. This may be attributed to the non-monotonic trend observed in the normalised growth rate as α increases. Note that TAN_z, the contribution to KIN by the work done by the velocity and stress perturbations in the spanwise direction at each α, is negative. Also the total negative contribution to KIN in the slip case is higher than that in the no-slip case; however, the positive contribution from TAN_x in the no-slip case is more than that for slip case. This results in larger growth rate for the no-slip case at each α.

However, a configuration with high viscous ($m = 30$), low density fluid ($r = 0.5$) in the lower layer is more linearly unstable to three-dimensional disturbances ($\Omega_i/\Omega_{i2D} > 1$) in a window $(0, \beta_s)$ of β values, for all combinations of velocity slip parameters considered (see Fig. 4(a)). Here, β_s is that value of β beyond which $\Omega_i/\Omega_{i2D} < 1$, for each combination of slip parameters at the walls. The other parameters are $Re = 100$, $\alpha = 0.5$, $G = -0.01$ and $\Gamma_{ic} = 0.1$. This occurs for $h_l = 0.5$. Also, note that the maximum normalized growth rate occurs for this flow configuration in a channel with velocity slip at the lower wall and no-slip at the upper wall ($\beta_1 = 0$ and $\beta_2 = 0.05$). Further, the bandwidth of wave numbers for which the flow is unstable is larger for this configuration as compared to that for the no-slip case. From Fig. 4(c), we infer that the three-dimensional perturbations are dominant at large wavelengths, in a configuration that hosts high viscous, low density fluid in the lower layer, for all the types of slip conditions considered and this is in contrast to what is observed for the configuration hosting a high viscous and high density fluid in the lower layer. A careful inspection of Figs. 4(a), (c) and (d) reveal that, as the wave number increases, the three-dimensional disturbances remain dominant (at moderate wave numbers Fig. 4(a)). With further increase in α (Fig. 4(c)), the two-dimensional disturbances become dominant in the short-wave regime. With a decrease in viscosity contrast ($m = 20$), keeping the other parameters the same, we can see that $\Omega_i/\Omega_{i2D} > 1$ in a β-window (β_l, β_s) where for $\beta < \beta_l$ and $\beta > \beta_s$, $\Omega_i/\Omega_{i2D} < 1$, for each combination of velocity slip at the walls

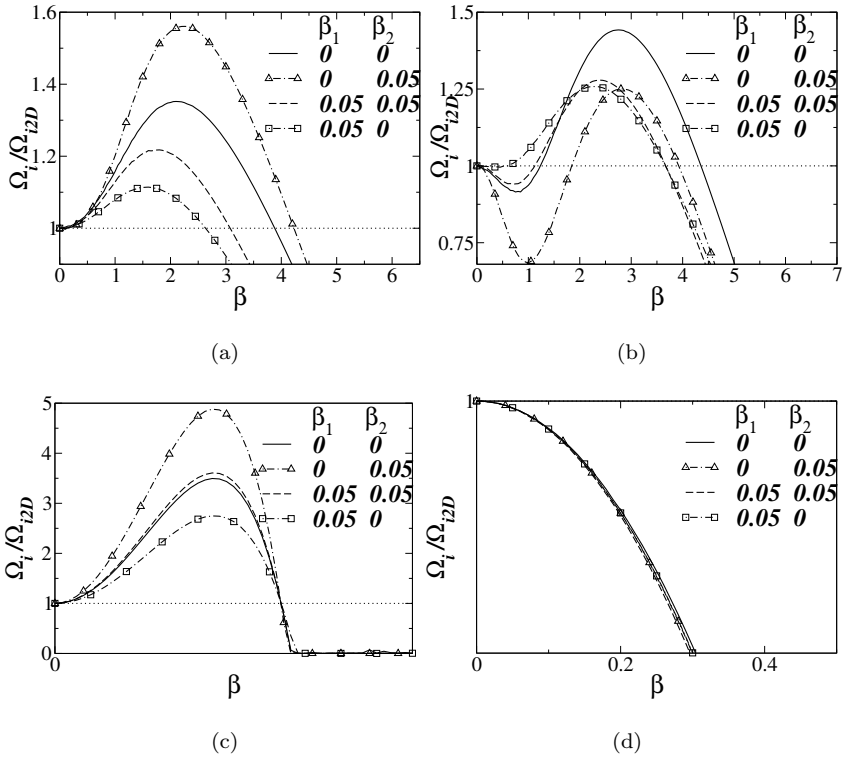

Figure 4: The effects slip parameters on the normalized growth rate, Ω_i/Ω_{i2D} as a function of spanwise wave number β for a system with high viscous, low density lower layer. (a) $m = 30$ and (b) $m = 20$ when $\alpha = 0.5$. For $m = 30$, the slip effects on the growth rate at the long wave (c) $\alpha = 0.001$ and in the short wave regime (d) $\alpha = 10$ are plotted. The rest of the parameters are $Re = 100$, $h_l = 0.5$, $r = 0.5$, $G = -0.01$ and $\Gamma_{ic} = 0.1$.

of the channel (Fig. 4(b)). We observe that, for this set of parameters, the maximum normalized growth rate occurs in a rigid channel.

In order to show that the most unstable mode in the slip case is an interfacial mode as observed in case of no-slip (Sahu and Matar, 2011), we plot the eigenfunctions of the most unstable mode for $\beta_1 = 0$ and $\beta_2 = 0.05$ in Fig. 5. It can be clearly seen that this is an interfacial mode with a sudden jump occurring at the interface (in this figure $y = 0.5$). We find the same conclusion for other parameters considered in the present study.

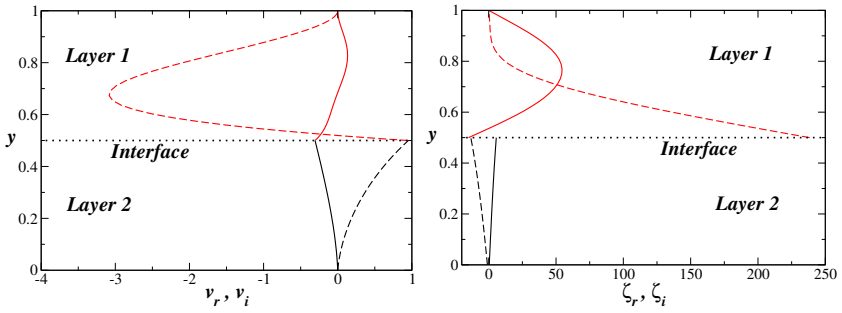

(a) (b)

Figure 5: The real (solid line) and imaginary (dashed line) parts of the eigenfunctions v (panel a) and ζ (panel b) associated with the most unstable mode ($\beta = 2.2$) in each layer for $\beta_1 = 0$ and $\beta_2 = 0.05$. The rest of the parameters are the same as those used to generate Fig. 4.

If the depth of the lower layer is increased ($h_l = 0.6$), for $m = 20$, with other parameters kept fixed, temporal linear instability is dominated by two-dimensional disturbances, for all combinations of slip conditions (Fig. 6(a); at a moderate wave number, $\alpha = 0.5$). On the other hand at this wave number ($\alpha = 0.5$), when viscosity stratification is increased ($m = 30$), the three-dimensional

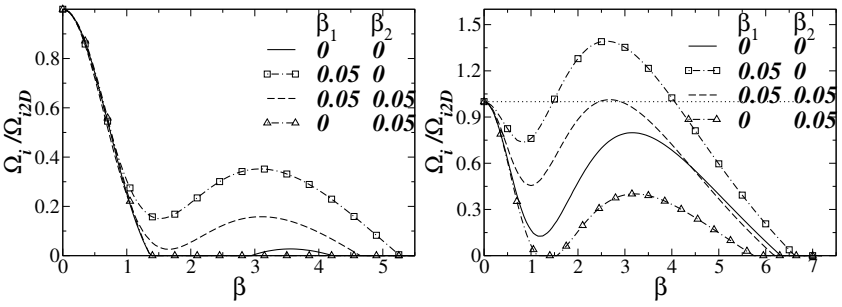

(a) (b)

Figure 6: The effects slip parameters on the normalized growth rate, Ω_i/Ω_{i2D} as a function of spanwise wave number β for a configuration hosting high viscous, low density lower layer. (a) $m = 20$ and (b) $m = 30$. The rest of the parameters are $Re = 100$, $h_l = 0.6$, $\alpha = 0.5$, $r = 0.5$, $G = -0.01$ and $\Gamma_{ic} = 0.1$.

disturbances dominate in a $\beta-$window (β_l, β_s) for the cases with $\beta_1 = \beta_2 = 0.05$ and with $\beta_1 = 0.05$, $\beta_2 = 0$ (Fig. 6(b)). The computations for the long and short wave lengths reveal that the three-dimensional (two-dimensional) disturbances are dominant at the long wave lengths (short wave lengths) and the behaviour is similar to that in Figs. 4(c), (d) for all types of slip conditions (figure not shown).

3.2. Spatio-temporal analysis

The above results are based on a temporal stability analysis in which the wave number is constrained to be a real number (i.e. only waves that do not grow or decay in the streamwise direction is considered) and whether such waves grow or decay in time is examined. In what follows, we have examined the absolute and convective instabilities of the linear dynamics by performing a spatio-temporal analysis in a two-fluid configuration in a channel with no-slip at the bottom wall and slip at the top surface. In a spatio-temporal stability analysis, the wave number and the frequency are both allowed to be complex numbers (Briggs, 1964, Huerre, 2000, Huerre and Monkewitz, 1990). In this analysis, we try to understand how the linear system responds; that is, we observe the evolution of the wave packet that results due to exciting every wave simultaneously with a small localized impulsive disturbance imposed on the liquid-liquid interface.

The focus is only on waves that satisfy the dispersion relation. These waves propagate away from the source of disturbance. The waves have different velocities, dictated by their group velocity $d\Omega/d\alpha$. The rate of growth or decay is different and is dictated by their growth rate. The flow is stable, if each wave decays in time and unstable if some waves grow in time. The system is convectively unstable or the system is a spatial amplifier if the perturbation grows as it is convected away from the point of initiation of the impulse, i.e. if the long time behaviour decays along $x/t = 0$. If there is growth of the perturbation at every point, then the system is absolutely unstable or the system acts like oscillators (Duprat et al., 2007, Huerre and Monkewitz, 1990).

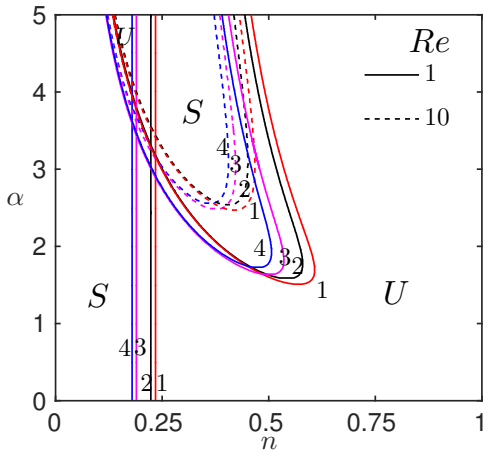

Figure 7: Neutral stability boundaries for two-dimensional disturbances ($\beta = 0$) in α (the wave number of the disturbance)$-n$ (the ratio of thickness of layers) plane when the viscosity ratio $m = 0.05$, in a density matched (density ratio, $r = 1$) two-layer configuration in a rigid/slippery channel. The solid curves are for $Re = 1$ and the dashed curves are for $Re = 10$. Curves marked as 1, 2, 3 and 4 correspond to the results with boundary conditions $\beta_1 = 0$ and $\beta_2 = 0.05$, $\beta_1 = 0$ and $\beta_2 = 0$, $\beta_1 = 0.05$ and $\beta_2 = 0.05$, and $\beta_1 = 0$ and $\beta_2 = 0.05$, respectively.

The complex dispersion relation obtained by solving the eigenvalue problem (Eqs. (24)$-$(36)) numerically for a range of complex wave numbers, $\alpha = \alpha_r + i\alpha_i$ is used to determine the spatio-temporal behaviour of the instability. If α_s is the wave number (α) at which the group velocity $d\Omega/d\alpha = 0$, then the necessary condition for the flow to be absolutely unstable is that the imaginary part $\Omega_{i,0}$ of the angular frequency $\Omega_i(\alpha_s)$ must be positive at a saddle point α_s in the complex $\alpha_i - \alpha_r$ plane (Huerre and Monkewitz, 1990). The sufficient condition is fulfilled if there is a formation of cusp branch point at $\Omega_{i,0}$ in the $\alpha_i - \alpha_r$ plane (a genuine pinch point), which corresponds to coalescence at the saddle point α_s of the branches originating from opposite halves of the $\alpha_i - \alpha_r$ plane. When both the necessary and sufficient conditions are satisfied, then the perturbation at the point of initiation of the disturbance grows with absolute growth rate $\Omega_{i,0}$.

The results of a spatio-temporal Orr-Sommerfeld-Squire analysis are presented in this section and the nature of instability is assessed. The choice of the range of parameters for the computations is motivated by the results in Fig. 7. In Fig. 7, the neutral boundaries are plotted for different combinations of slip conditions in a two-layer configuration in a rigid/slippery channel and the influence of inertia is assessed. An increase in Reynolds number from $Re = 1$ (solid curves) to $Re = 10$ (dashed curves) is destabilizing the flow in a slippery channel hosting a less viscous fluid ($m = 0.05$) in the lower layer. This is similar to the results associated with a rigid channel presented by Yiantsios and Higgins (see figure 5 in Ref. Yiantsios and Higgins (1988)) with the other parameters the same as in Fig. 7). In the no-slip case, the stable region is shifted to higher wave numbers for $n^2 > m$. For all other types of slip boundary conditions ($\beta_1 = 0$ and $\beta_2 \neq 0$, $\beta_1 \neq 0$ and $\beta_2 = 0$, and $\beta_1 \neq 0$ and $\beta_2 \neq 0$), this happens for $n(n + 2\beta_2) > m(1 + 2\beta_1)$.

Further, for $Re = 1$ and $Re = 10$, for the system with stronger velocity slip at the lower wall ($\beta_1 = 0$ and $\beta_2 = 0.05$), the stable region is shifted towards higher values of thickness ratio (n) as compared to that for no-slip case ($\beta_1 = 0$ and $\beta_2 = 0$), and the reverse is seen for symmetric slip ($\beta_1 = \beta_2 = 0.05$) and stronger slip at the upper wall ($\beta_1 = 0.05$ and $\beta_2 = 0$). Thus, the Reynolds number is destabilizing for all types of wall boundary conditions considered. In view of the above results and remarks on Squire's theorem and squire transformation presented in section 1, the parameter regime where Squire's theorem fails are considered and the results are obtained.

The isocontours of Ω_r (spatial amplification rate) and Ω_i (angular frequency) are plotted (not shown) for two-dimensional disturbances when $\beta = 0$ and for three-dimensional disturbances when $\beta = 2$ for the flow in a rigid channel. The parameters considered are $Re = 500$, $h_l = 0.3$, $m = 30$, $r = 1.2$, $\Gamma_{ic} = 0.01$ and $G = 10$ (these are the same as in Sahu and Matar (2011)) and they agree with Valluri et al. (2010) for two-dimensional disturbances ($\beta = 0$) and with Sahu and Matar (2011) for three-dimensional disturbances ($\beta = 2$) for the flow in a rigid channel.

Table 2: The Reynolds number (Re^*) at which the transition from convective to absolute instability occurs for slip/no-slip boundary conditions.

Boundary conditions	Re^*
$\beta_1 = 0, \beta_2 = 0$	55.626
$\beta_1 = 0.05, \beta_2 = 0$	55.833
$\beta_1 = 0.05, \beta_2 = 0.05$	63.445
$\beta_1 = 0, \beta_2 = 0.05$	63.195

Next, the effects of velocity slip at the walls of the channel on the spatial growth rates are investigated. There are several spatial branches in the complex $\alpha_i - \alpha_r$ plane with $\Omega_i = 0$. The Reynolds number at which the spatial branch emanating from $\alpha_i = 0$ coalesces with another spatial branch in the lower half of the $\alpha_i - \alpha_r$ complex plane (denoted by Re^*) is presented in Table 2, for each type of slip boundary conditions considered in this study. This occurs at a saddle point at which there is transition to absolutely unstable flow from convective instability. The results show the details for the configuration with high viscous ($m = 30$), isodense ($r = 1$) fluid in the layer adjacent to the lower wall. The other parameters are fixed as $\Gamma_{ic} = 0.01$, $h_l = 0.3$, $G = 0$ and $\beta = 0$. The results match well with Valluri et al. (2010) (see figure 2(d) in Ref. Valluri et al. (2010)), for the no-slip case. The computations further reveal that the interface is convectively unstable for $Re < Re^*$ in each case. It is clear that the occurrence of this transition is delayed due to velocity slip at the upper wall and no-slip at the lower wall (adjacent to which the high viscous fluid is placed) and the same is further delayed, when there is symmetric slip at the walls or stronger slip at the lower wall. Having validated the results in a rigid channel using the developed code, the computations are performed to understand the spatio-temporal stability characteristics in a slippery channel.

In what follows, all the computations for the spatio-temporal analysis have been presented for the configuration with slip at the upper wall and no-slip

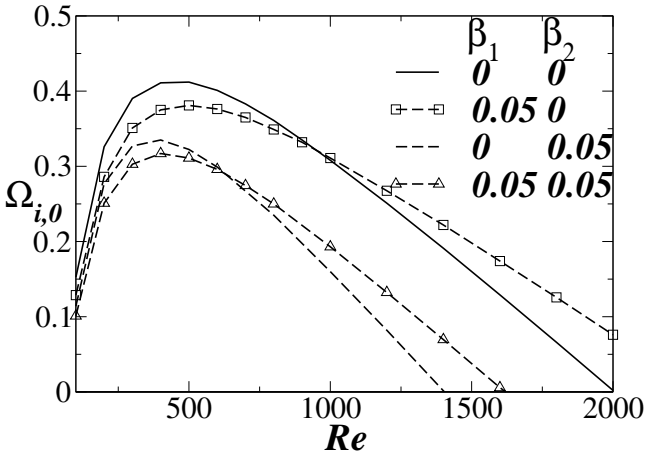

Figure 8: The effects of velocity slip on the absolute growth rate ($\Omega_{i,0}$) for three-dimensional disturbance ($\beta = 1$) as a function of the Reynolds number (Re). The rest of the parameters are $m = 30$, $r = 0.5$, $h_l = 0.3$, $G = -0.01$ and $\Gamma_{ic} = 0.1$.

at the lower wall ($\beta_1 = 0.05, \beta_2 = 0$). This choice has been motivated by the results shown in Fig. 8. The isocontours of Ω_r and Ω_i have been plotted (figure not shown) for three-dimensional disturbances ($\beta = 1$) for different slip boundary conditions at the channel, namely (a) symmetric slip: $\beta_1 = \beta_2 = 0.05$; (b) velocity slip at the lower wall and no-slip at the upper wall: $\beta_1 = 0$ and $\beta_2 = 0.05$, and (c) the slip at the upper wall and no-slip at the lower wall: $\beta_1 = 0.05$ and $\beta_2 = 0$ for a two-layer configuration with high viscous ($m = 30$) and low density ($r = 0.5$) fluid near the lower wall. The liquid-liquid interface is far away from the upper wall ($h_l = 0.3$). The other parameters are fixed at $G = -0.01$ and $\Gamma_{ic} = 0.1$. The absolute growth rates ($\Omega_{i,0}$) are extracted. Fig. 8 presents these results for the above slip boundary conditions along with that for no-slip ($\beta_1 = \beta_2 = 0$) at both the walls. We observe the dominance of $\Omega_{i,0}$ for the case with velocity slip at the upper wall and no-slip at the lower wall (case (c) described above) over those of the other two types of slip boundary conditions (cases (a) and (b) described above). In view of this, the computations are performed only for the slip condition (case (c)) for which the absolute growth rate is maximum for the set of parameters considered.

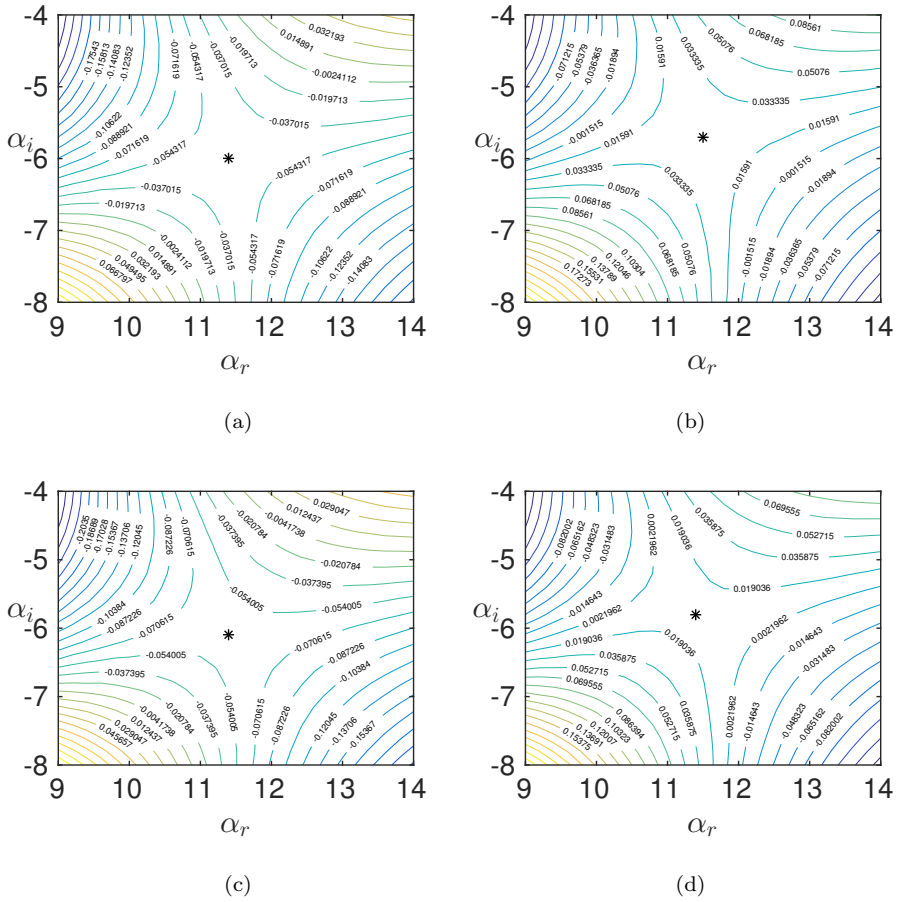

Figure 9: The isocontours of Ω_i in the complex wave number plane for (a) $\beta_1 = 0$ and $\beta_2 = 0$ (no-slip case), two-dimensional disturbance ($\beta = 0$), (b) $\beta_1 = 0.05$ and $\beta_2 = 0$ (slip at the upper wall and no-slip at the lower wall), two-dimensional disturbance ($\beta = 0$), (c) $\beta_1 = 0$ and $\beta_2 = 0$ (no-slip), three-dimensional disturbance ($\beta = 1$) and (d) $\beta_1 = 0.05$ and $\beta_2 = 0$ (slip at the upper wall and no-slip at the lower wall), three-dimensional disturbance ($\beta = 1$). Here, $m = 22$, $r = 0.5$, $Re = 1000$, $\Gamma_{ic} = 0.1$, $G = -0.01$ and $h_l = 0.3$.

Fig. 9 presents the isocontours of imaginary part of Ω (Ω_i) for a flow system hosting a high viscous ($m = 22$), low density ($r = 0.5$) fluid in the lower layer for $Re = 1000$, $\Gamma_{ic} = 0.1$, $G = -0.01$ and $h_l = 0.3$. At the saddle point, $\Omega = 4.28 - i0.048$ in the absence of velocity slip ($\beta_1 = 0$ and $\beta_2 = 0$; Fig.

9(a)) and $\Omega = 3.71 + i0.025$ for $\beta_1 = 0.05$ and $\beta_2 = 0$ (see Fig. 9(b)) for the two-dimensional disturbances ($\beta = 0$). The corresponding Ω for the three-dimensional disturbances ($\beta = 1$) are $\Omega = 4.27 - i0.06$ for the no-slip boundary condition at both the walls (Fig. 9(c)) and $\Omega = 3.7 + i0.015$ for the case of slip at the upper wall and no-slip at the lower wall (Fig. 9(d)). We observe, for this set of parameters, the flow system which was otherwise convectively unstable in the absence of velocity slip, becomes absolutely unstable due to velocity slip at the upper wall. This scenario is observed for both two and three-dimensional perturbations. The absolute growth rate $\Omega_{i,0}$ is dominant for two-dimensional disturbances in the presence of velocity slip.

Further, the amplification rate, $\Omega_{r,0}$ decreases with increase in the value of velocity slip for both two and three-dimensional perturbations, and it is higher for two-dimensional disturbances in the absence of slip. It is evident from Fig. 10 that the inertial effects enhance $\Omega_{r,0}$ for both two and three-dimensional disturbances. At any Re, velocity slip lowers the amplification rate. The value of $\Omega_{r,0}$ is higher for two-dimensional disturbance in systems with no-slip at both the walls, and slip at upper wall and no-slip at the lower wall.

The influence of the location of the interface as it is moved towards the wall with slip (upper), on absolute growth rate is assessed and the curves of zero absolute growth rate ($\Omega_{i,0} = 0$) are presented in Fig. 11. Here, the dashed lines correspond to $\beta_1 = 0.05$ and $\beta_2 = 0$ and the solid lines correspond to $\beta_1 = 0$ and $\beta_2 = 0$ respectively. They separate the regions where the flow is convectively unstable and regions where the flow is absolutely unstable in the $h_l - Re$ parameter space, for a configuration with high viscous ($m = 30$), low density ($r = 0.5$) fluid near the lower wall without velocity slip. The other parameters are fixed at $G = -0.01$ and $\Gamma_{ic} = 0.1$. The configuration is convectively unstable for moderate to high film thickness ratio for the range of the Reynolds numbers considered. This regime is reduced by the presence of slip at the upper wall ($\beta_1 = 0.05$ and $\beta_2 = 0$); this results in enhancement of absolutely unstable regime in $h_l - Re$ parameter space for a system with velocity slip at the upper wall. Thus, there is a critical film thickness ratio (h_{lc}) (in the small

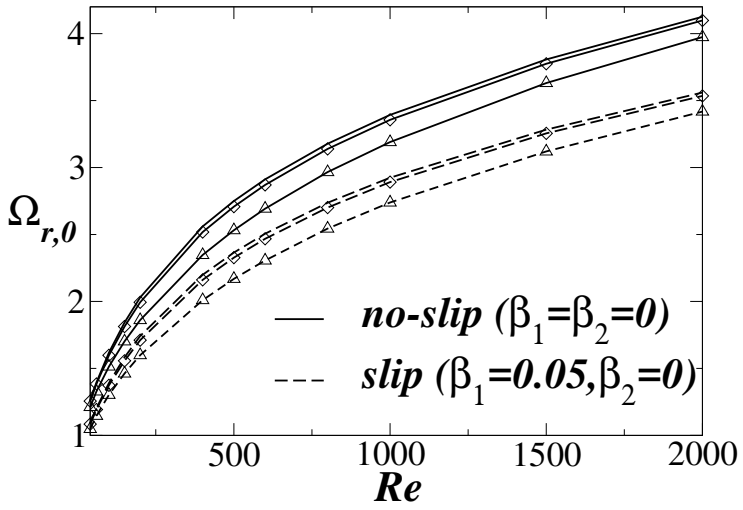

Figure 10: The effects of velocity slip on the amplification rate ($\Omega_{r,0}$) as a function of the Reynolds number (Re) for two ($\beta = 0$; no symbol) and three-dimensional disturbances ($\beta = 2$: diamond, $\beta = 5$: triangle($\triangle$)). The solid and the dashed lines present the results for the no-slip at both the walls, and the slip at the upper wall with no-slip at the bottom wall, respectively. The lower layer hosts a high viscous ($m = 30$), low density ($r = 0.5$) fluid. The rest of parameters are $h_l = 0.3$, $G = -0.01$ and $\Gamma_{ic} = 0.1$.

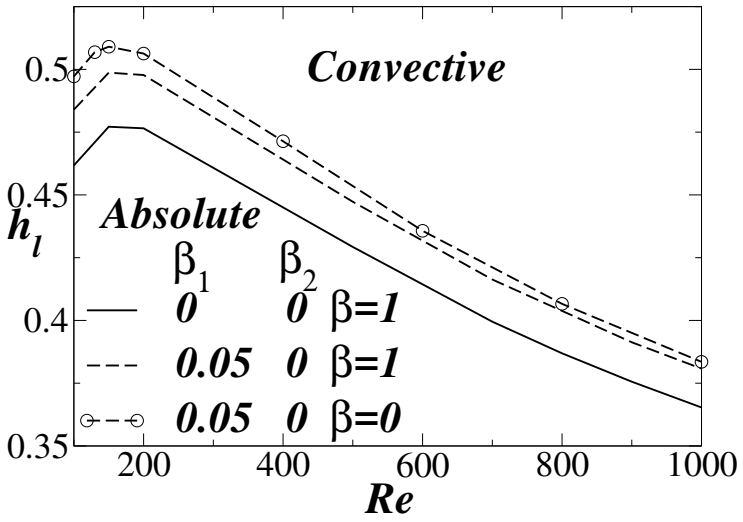

Figure 11: The absolutely and convectively unstable regions in the $h_l - Re$ space for the two ($\beta = 0$) and three dimensional ($\beta = 1$) disturbances. The rest of the parameters are $m = 30$, $r = 0.5$, $G = -0.01$ and $\Gamma_{ic} = 0.1$.

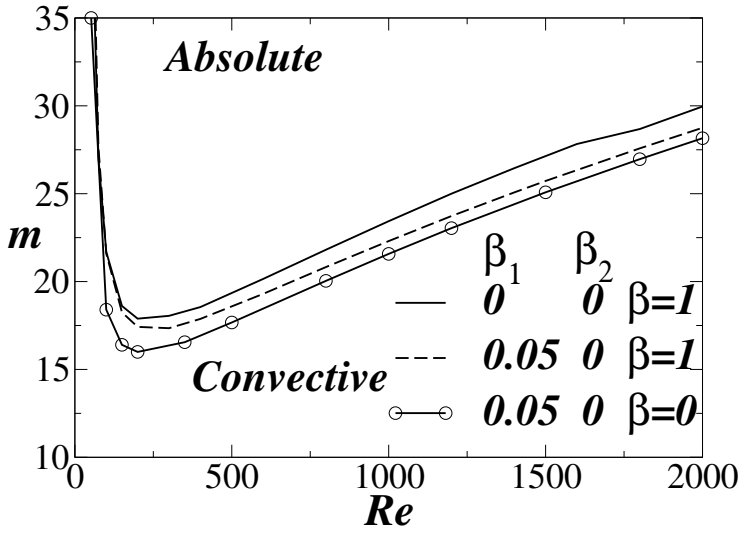

Figure 12: The absolute and convective unstable regions separated by zero contours of absolute growth rate in $m-Re$ parameter regime for the two ($\beta = 0$) and the three dimensional ($\beta = 1$) disturbances. The rest of the parameters are $h_l = 0.3$, $r = 0.5$, $G = -0.01$ and $\Gamma_{ic} = 0.1$.

to moderate values range) below which this system is absolutely unstable at any fixed Reynolds number and this is extended to high Reynolds number also. Further, note that (h_{lc}) in the presence of slip at the upper wall is greater than (h_{lc}) for the no-slip case. This can be exploited in designing the walls of the channel as walls with velocity slip when one deals with an inertia dominated system having moderate thickness ratios of the two-layers. The two-dimensional perturbations (dashed lines with circles; $\beta = 0$) are more absolutely unstable at small to moderate Reynolds numbers than the corresponding three-dimensional disturbance in a channel with slip at the upper wall.

In Fig. 12, the boundaries separating the convectively and absolutely unstable regions in $m - Re$ parameter regime are shown, for a thinner lower layer hosting high viscous low density fluid. The other parameters are the same as in Fig. 11. In the region above the boundary, (solid curve: $\beta_1 = \beta_2 = 0$; dashed curve: $\beta_1 = 0.05$ and $\beta_2 = 0$), the base flow is absolutely unstable for $h_l = 0.3$, $r = 0.5$, $G = -0.01$, $\beta = 1$ and $\Gamma_{ic} = 0.1$. Thus, absolute instability prevails

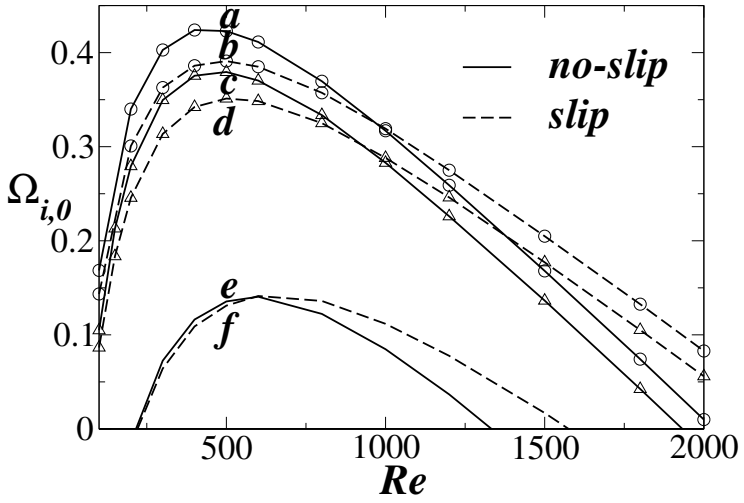

Figure 13: The variation of the absolute growth rate ($\Omega_{i,0}$) versus the Reynolds number (Re). The no-slip ($\beta_1 = 0$ and $\beta_2 = 0$): solid lines, and slip case ($\beta_1 = 0$ and $\beta_2 = 0.05$): dashed line. $\beta = 0$: circles, and $\beta = 2$: upward triangle, $\beta = 5$: no symbol. The rest of the parameters are $h_l = 0.3$, $m = 30$, $r = 0.5$, $\Gamma_{ic} = 0.1$ and $G = -0.01$.

in the $m - Re$ parameter space for moderate to high viscosity contrasts at all Reynolds numbers, with an exception of a narrow window at low Reynolds numbers. At small to moderate viscosity contrasts, the flow is convectively unstable and an increase in the inertial effects result in a higher viscosity contrast configuration to be absolutely unstable. The presence of velocity slip ($\beta_1 = 0.05$ and $\beta_2 = 0$) enlarges the region of absolute instability for both the two and the three-dimensional disturbances. In other words, the flow configuration which was otherwise convectively unstable (no-slip at the walls) for the range of m and Re, becomes absolutely unstable in the presence of velocity slip at the upper wall (the corresponding region is the strip bounded between the solid ($\beta_1 = 0$ and $\beta_2 = 0$) and the dashed ($\beta_1 = 0.05$ and $\beta_2 = 0$) curves in Fig. 12). As in Fig. 11, the $m - Re$ regions where absolute instability prevails, is larger for the two-dimensional disturbances ($\beta_1 = 0.05$ and $\beta_2 = 0$, solid curve with circle) than for the three-dimensional disturbances ($\beta_1 = 0.05$, $\beta_2 = 0$, dashed curve without symbols).

Table 3: Energy Budget for points labelled a, b, c, d, e, f in Fig. 13.

Point	REY_2	REY_1	DIS_2	DIS_1	TAN_x	TAN_z	TEN	HYD
a	0	0.0078	-0.0116	-0.0178	1.0216	0	0	0
b	0	0.0072	-0.0109	-0.0180	1.0217	0	0	0
c	0	0.0087	-0.0121	-0.0180	1.0221	-0.0006	0	0
d	0	0.0080	-0.0113	-0.0181	1.0221	-0.0006	0	0
e	0	0.0117	-0.0136	-0.0193	1.0243	-0.0031	0	0
f	0	0.0111	-0.0126	-0.0195	1.0239	-0.0029	0	0

Fig. 13 ($h_l = 0.3$, $m = 30$, $r = 0.5$, $\Gamma_{ic} = 0.1$ and $G = -0.01$) presents the inertial effects on the absolute growth rate ($\Omega_{i,0}$) at the saddle point (α_s), both for the no-slip ($\beta_1 = 0$ and $\beta_2 = 0$) and the case with velocity slip at the upper wall ($\beta_1 = 0.05$ and $\beta_2 = 0$). This plot clearly shows the stabilizing role of slip at the upper wall of the channel at small to moderate Reynolds numbers. There is a window of Reynolds numbers $(0, Re_u)$, for which the absolute growth rate for the flow configuration with no-slip is larger than that for the slip case; beyond Re_u, however, the trend is reversed due to the inertial effects. A decrease in spanwise wave number β increases Re_u, where this change occurs. In addition, beyond this Re_u, the absolute growth rate for the slip case is larger for both two and three-dimensional disturbances. Also, the absolute growth rate for the two-dimensional disturbances in a system with slip at the upper wall is larger than that for the three-dimensional disturbances with and without slip. Further, we observe that the absolute growth rate decreases as β increases (for both slip and no-slip cases). This indicates that in the parameter regime of absolute instability of the systems with or without velocity slip, the most unstable two-dimensional disturbance dominates the corresponding three-dimensional perturbations near the onset, in spite of fact that the three-dimensional disturbances are more temporally unstable.

The energy budget analysis reveals that (Table 3) at each β, the negative contribution from DIS terms and the positive contributions from the TAN_x and REY_1 terms in the energy budget, to KIN are more in the no-slip case as compared to the slip case indicating larger absolute growth rate at this Re (= 500) for the no-slip case. Further, as β increases, both the positive and negative contributions to KIN increase, resulting in decrease in absolute growth rate as β increases. This indicates that two-dimensional disturbances ($\beta = 0$) are dominant in the spatio-temporal analysis. Further, as before, TAN_x has larger positive contribution to KIN both for $\beta = 0$ and $\beta \neq 0$, showing that the unstable mode is the interface mode for both two and three-dimensional perturbations. As a result, the dominant mode is the interface mode arising due to two-dimensional perturbations.

The results from Figs. 11, 12 and 13 provide the essence of the present investigation and hence merits further emphasis. The parameter regimes which were

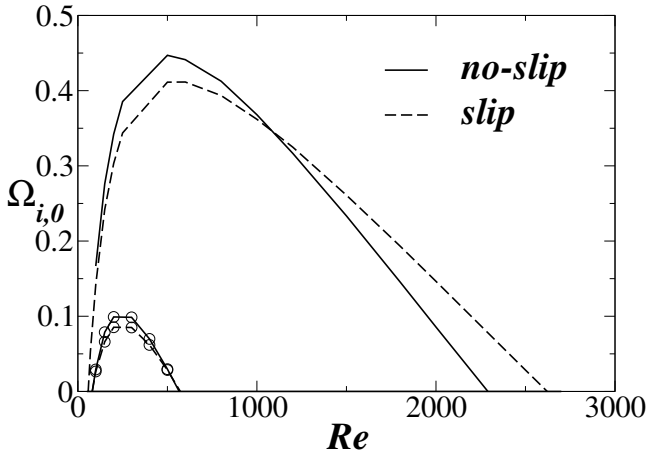

Figure 14: Effects of surface tension and velocity slip on the variation of absolute growth rate, $\Omega_{i,0}$ as a function of the Reynolds number. The rest of the parameters are fixed at $h_l = 0.3$, $m = 30$, $r = 1$, $G = 0$, $\beta = 0$ (two-dimensional disturbance), $\Gamma_{ic} = 0.1$ (no symbol), $\Gamma_{ic} = 10$ (circle). The results for no-slip case ($\beta_1 = 0$ and $\beta_2 = 0$; solid lines) correspond to those in Valluri et al. (2010). The results for velocity slip at the upper wall ($\beta_1 = 0.05$ and $\beta_2 = 0$) are presented with dashed lines.

otherwise convectively unstable become absolutely unstable for a system with slip with respect to three-dimensional perturbations and this region is further enlarged for all Reynolds numbers with respect to two-dimensional disturbances.

In what follows, we consider the effects of surface tension on the absolute growth rate of two-dimensional disturbances. Fig. 14 ($m = 30$, $r = 1$, $h_l = 0.3$, $G = 0$ and $\beta = 0$) shows that surface tension has a strong stabilizing effect; the absolute growth rate associated with the two-dimensional disturbances decreases significantly with an increase in surface tension both for the no-slip case as considered by Valluri et al. (2010) and the slip case (present study). Under weak surface tension, ($\Gamma_{ic} = 0.01$), there is a decrease in $\Omega_{i,0}$ in a window of small to moderate Reynolds numbers (say, Re_m), but beyond Re_m, $\Omega_{i,0}$ is larger for a fixed value of Re in the presence of the velocity slip. However, when the surface tension is strong ($\Gamma_{ic} = 10$), the velocity slip facilitates a decrease in the value of $\Omega_{i,0}$ and the bandwidth of Re with absolute growth rate, $\Omega_{i,0}(> 0)$ is significantly reduced with and without the presence of the velocity slip.

4. Discussion

Fig. 13 shows that the absolute growth rates corresponding to the two-dimensional disturbances are larger than that for the three-dimensional perturbations, indicating that the two-dimensional modes might dominate the three-dimensional modes close to the instability threshold, for the parameters values considered in the present investigation. Further, note that the Reynolds number, based on the mean velocity U_m is influenced by the presence of velocity slip. This may be responsible for larger disturbance growth rates in the presence of slip manifested as effects of advection, thus enhancing the perturbation amplitude locally near the point of perturbation. As a result, the absolutely unstable region (instability due to three-dimensional perturbations) in the $m - Re$ parameter regime is larger in a system with slip at the channel walls. This region is further enlarged in a channel with slippery walls, wherein the instability arises due to two-dimensional disturbances. We also observe that for small and very

large Reynolds numbers, the rate of growth of the perturbation is dominated by the rate of advection due to which the system is convectively unstable. A careful observation of Fig. 13 reveals that the absolute growth rate increases with decrease in β both for no-slip and slip at the channel walls in a window of small to moderate Reynolds numbers. For each β, there is a cut-off Reynolds number, $Re(\beta)$ upto which the absolute growth rate for a configuration with no-slip exceeds that for the corresponding system with slip at the wall (stabilizing role of velocity slip). This may be attributed to enhanced rate of energy transfer from the base state to the perturbations arising due to stresses in the upper layer. Beyond $Re(\beta)$, a reverse trend is observed (destabilizing role of velocity slip) and may be attributed to the inertial effects. This clearly brings out the non-monotonic trend in the absolute growth rate with respect to velocity slip, and this suggests that the instabilities can be either suppressed or promoted by the wall slip and is dependent on the inertial effects, viscosity contrast and thickness ratio. Further, we note that the stability characteristics in a system with slip resembles those in a system with no-slip boundary condition; thereby indicating that there is no new physical mechanism introduced due to the slip at the wall, that is responsible for the instabilities in a channel flow. Note that, this is not an obvious conclusion at first sight but is an outcome of a detailed and thorough analysis performed in the previous sections. It is clear that the curvature jump of the base state velocity profile at the interface (Fig. 2) arises due to density contrast ($r = 0.5$) between the two layers. This, in turn introduces shear-stress disturbances tangential to the interface so as to maintain continuity of total shear stress. As a consequence, there may be a significant contribution to the rate of energy transfer due to the perturbations in shear stresses in the upper layer located near the wall with velocity slip.

The energy budget details presented by Sahu and Matar (2011) reveal that the largest contribution to the spatially averaged rate of change of kinetic energy of the perturbations is from the work done by the stresses tangential to the interface. This confirms that the interface mode is the most dangerous one in the no-slip case. The above discussion and the results obtained from the energy

budget analysis in the present study clearly indicate that the interface mode is the dominant mode in a two-fluid flow system with slip at the upper wall and no-slip at the lower wall. Further, as in the no-slip case, the two-dimensional disturbances are expected to be dominant as compared to three-dimensional disturbances at the onset of instability.

In addition, the present investigation is motivated by some practical problems in which the practice is to displace the more viscous fluid (such as viscous soils in industrial plant) which completely fills the pipeline initially, by water during cleaning and product turnover operations. This causes the viscous films to be left behind on walls of the pipe by finger of water. This mimics a two-layer system in a confined channel with the two-fluids having different physical properties, namely, different viscosities and/or densities. Although non-Newtonian fluids are susceptible to velocity slip at the walls of the channel, investigations on displacement of Newtonian fluids is crucial and important as both the fluids demonstrate some common qualitative behaviours and it is easier to understand these features when one works with Newtonian fluids. Due to relevance of wall slip velocity (as mentioned in Introduction), the present study considers stability of Poiseuille flow of a two fluid system in a slippery channel. At this stage, it is worth mentioning about the investigation by Taghavi (2018) on a two-layer model for buoyant displacement flows of generalised Newtonian fluids in a channel with wall slip. He has also considered different combinations of slip conditions at the walls as in the present study. Although the configuration considered is "displacement" and not "stratified" flows, there are some similarities between the present study and the work of Taghavi (2018). In the displacement flow addressed by Taghavi (2018), slip at either wall has significant influence on the overall displacement but the efficient displacements have been found for the scenario, where there is wall slip at the upper wall and no-slip at the lower wall. In the present study, where stratified flow is considered, it has been observed that the case with wall-slip at the upper wall has more absolute growth rate in some parameter regimes than the no-slip/other type of wall slip conditions considered. While absolute growth rate demonstrates a non-monotonic trend

with respect to slip at the upper wall both for two and three-dimensional disturbances (stratified flow in the present study), Taghavi's (2018) displacement flow study reveals such a trend for the heights and speeds of the leading and trailing fronts as functions of viscosity ratio/buoyancy number.

The discussion would be incomplete if there is no mention about how experiments can be designed and performed in order to compare against the theoretical results observed in the present study. The experimental set up in laboratory scale must be such that there should be well-controlled wall slip at the walls of the channel. Lauga and Stone (2003), Nickerson and Kornfield (2005) and Vayssade et al. (2014) have provided experimental techniques that would help to characterize slip or control the occurrence of slip in small flow systems. Recently, Taghavi (2018) has pointed out a possible way of setting up an experiment by hosting a low viscous fluid in a very thin layer (that may serve as a lubricant) adjacent to a wall; the velocity slip at the wall results from a micro scale description of the boundary condition at the layer. There are methods for hydrophobizing the walls of channels and pipes (Churaev et al., 1984).

5. Concluding remarks

This investigation addresses a fundamental hydrodynamic stability problem in fluid mechanics regarding a two- layer channel flow with boundary slip. The wall slip mimics a hydrophobic surface which can have many applications in the light of turbulence control. The problem is formulated within the following framework: (i) general 3D Navier-Stokes equations for each layer assuming Newtonian fluids of varying density and/or viscosity, (ii) applying wall slip in the simple form of Navier-slip condition relating the fluid's speed at wall to local shear stress, (iii) perturbing the developed system, linearizing and assuming periodic temporal stability, and later spatio-temporal stability evaluating convective versus absolute instability conditions, (iv) assessing and comparing flow instability of Orr-Sommerfeld equations in two-dimensional and three-dimensional in the light of wall slippage degree, Reynolds number, viscosity

contrast, density contrast, and wave number. The computations have been carried out for parameters values where Squire's theorem fails (for two-layer flow configuration in a slippery channel). An eigenvalue problem governed by modified Orr-Sommerfeld and Squire systems along with boundary conditions is derived, incorporating velocity slip at the walls, by taking the disturbance frequency and wave number to be complex. The analysis, restricted to real wave number (temporal analysis) shows that the three-dimensional perturbations are more unstable than the corresponding two-dimensional perturbations. The velocity slip either promotes or suppresses the temporal growth rate and is influenced by the type of slip condition at the walls, the inertial effects, viscosity and density contrasts. The spatio-temporal stability analysis is carried out based on the Brigg's method for a two-layer configuration with no-slip at the lower wall and slip at the upper wall. The computations show that the two-dimensional modes are dominant near the onset of instability than the corresponding three-dimensional modes and that in a configuration with thinner lower layer, with decreasing viscosity and increasing density towards the wall with slip, there is an enlargement of absolutely unstable region (Fig. 12). As the interface moves nearer to the wall with slip, the absolute unstable region is enlarged for a configuration with wall slip (Fig. 11). Further, maximum absolute growth rate displays a non-monotonic trend with respect to slip at the upper wall and is influenced by the inertial effects for a configuration hosting a high viscous, low density fluid in the lower layer. The above results are similar to those observed in a double diffusive miscible system in a channel with slip at the wall (when destabilization occurs due to the slow diffusing species) by Ghosh et al. (2014a).

The role of velocity slip at a smooth surface in enhancing absolute instability in some parameter regime for a two-layer flow of immiscible fluids in a channel shows the path for achieving early transition to turbulence; namely, design the walls of the channel as substrates such as porous/rough/hydrophobic surfaces that can be modelled as smooth surfaces with slip at the walls.

Acknowledgement : We sincerely thank all the referees for their very valuable suggestions and comments. We also thank the editor of International Journal of Multiphase Flow for his very encouraging remarks.

Appendix A.

The variation of Ω_i/Ω_{i2D} versus α for different values of G is presented in Fig. A.15, for a configuration with high viscous ($m = 30$), low density ($r = 0.5$) fluid in the lower layer adjacent to a slippery wall ($\beta_1 = 0, \beta_2 = 0.05$). The other parameters are $Re = 100$, $h_l = 0.5$, $\alpha = 0.5$, $\Gamma_{ic} = 0.1$; these parameters are the same as in Fig. 4(a) for $\beta_1 = 0$ and $\beta_2 = 0.05$. The no-slip condition is imposed on the top wall. The results reveal that inclusion of gravity effects does not significantly change the normalised temporal growth rate for the range of parameters values considered. However, it can be observed that, as expected, decreasing the value of G increases the growth rate.

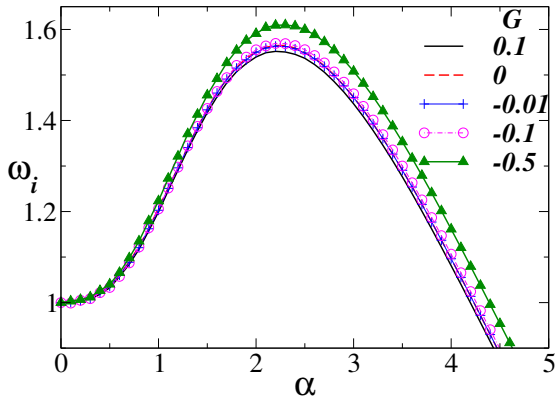

Figure A.15: Effect of G on the on the normalized growth rate, Ω_i/Ω_{i2D} as a function of spanwise wave number β for a system with highly viscous, low density fluid in the lower layer. The rest of the parameters are $Re = 100$, $h_l = 0.5$, $\alpha = 0.5$, $r = 0.5$, $m = 30$, $\Gamma_{ic} = 0.1$, $\beta_1 = 0$ and $\beta_2 = 0.05$. The parameters are the same as in Fig. 4(a) for $\beta_1 = 0$ and $\beta_2 = 0.05$.

Appendix B. Energy budget analysis

The details of the terms in the energy budget analysis performed in this study are as follows (Sahu and Matar, 2011).

The energy equation is derived by taking the inner product of the x-momentum, y-momentum and z-momentum equations for the perturbed variables in each layer with their respective perturbed velocity components. The resulting equation is then averaged over the wavelengths $\frac{2\pi}{\alpha}$ and $\frac{2\pi}{\beta}$ in the x and the z directions, respectively and integrated over the height of channel. This yields

$$\sum_{j=1}^{2} KIN_j = \sum_{j=1}^{2} DIS_j + \sum_{j=1}^{2} REY_j + INT, \tag{B.1}$$

where subscript $j = 1$ and $j = 2$ represent the upper and lower fluids, respectively. In Eq. (B.1), KIN_j, DIS_j and REY_j are

$$KIN_j = \frac{r_j}{l_1 l_2} \frac{d}{dt} \int_{a_j}^{b_j} dy \int_0^{l_2} dz \int_0^{l_1} dx \left[\frac{1}{2} \left(\hat{u}_j^2 + \hat{w}_j^2 + \hat{v}_j^2 \right) \right], \tag{B.2}$$

$$DIS_j = -\frac{1}{l_1 l_2 Re} \int_{a_j}^{b_j} dy \int_0^{l_2} dz \int_0^{l_1} \mu_j dx \Big[2 \left(\frac{\partial \hat{u}_j}{\partial x} \right)^2 + 2 \left(\frac{\partial \hat{w}_j}{\partial z} \right)^2 + 2 \left(\frac{\partial \hat{v}_j}{\partial y} \right)^2 +$$

$$\left(\frac{\partial \hat{u}_j}{\partial y} + \frac{\partial \hat{v}_j}{\partial x} \right)^2 + \left(\frac{\partial \hat{u}_j}{\partial z} + \frac{\partial \hat{w}_j}{\partial x} \right)^2 + \left(\frac{\partial \hat{w}_j}{\partial y} + \frac{\partial \hat{v}_j}{\partial z} \right)^2 \Big], \tag{B.3}$$

$$REY_j = \frac{r_j}{l_1 l_2} \int_{a_j}^{b_j} dy \int_0^{l_2} dz \int_0^{l_1} dx \left[-\hat{u}_j \hat{v}_j \frac{\partial U_{jB}}{\partial y} \right]; \tag{B.4}$$

for the lower fluid, $\mu_2 = m$, $r_2 = r$, $a_2 = 0$, $b_2 = h_l$ and for the upper fluid, $\mu_1 = 1$, $r_1 = 1$, $a_1 = h_l$, $b_1 = 1$. KIN_j is the spatially averaged rate of change of disturbance kinetic energy and is proportional to the growth rate. DIS_j is the viscous dissipation of energy and is always negative. $INT = NOR + TAN$ is related to the existence of an interface mode and is split into two terms NOR and TAN, and these are the work done by the velocity and stress disturbances in the directions normal and tangential to the interface, respectively. NOR is given by

$$NOR = \frac{1}{l_1 l_2 Re} \int_0^{l_2} dz \int_0^{l_1} dx [\hat{v}_1 \tau_1^{yy} - \hat{v}_2 \tau_2^{yy}]_{h_l}^0, \tag{B.5}$$

which is further decomposed into TEN and HYD, work done against the deformation of the interface due to interfacial tension and gravity, respectively:

$$NOR \equiv TEN + HYD, \tag{B.6}$$

where

$$TEN = \frac{1}{l_1 l_2 Re} \int_0^{l_2} dz \int_0^{l_1} dx \left[\hat{v}\Gamma_{ic}\left(h_{xx} + h_{zz}\right)\right]_{y=h_l}, \quad \text{and} \tag{B.7}$$

$$HYD = \frac{1}{l_1 l_2 Re} \int_0^{l_2} dz \int_0^{l_1} dx \left[\hat{v}Gh\right]_{y=h_l}. \tag{B.8}$$

TAN is also further decomposed into TAN_x and TAN_z, work done by the velocity and stress disturbances in the streamwise and spanwise directions, respectively:

$$TAN_x = \frac{1}{l_1 l_2 Re} \int_0^{l_2} dz \int_0^{l_1} dx [\hat{u}_1 \tau_1^{xy} - \hat{u}_2 \tau_2^{xy}]_{h_l}, \tag{B.9}$$

$$TAN_z = \frac{1}{l_1 l_2 Re} \int_0^{l_2} dz \int_0^{l_1} dx [\hat{w}_1 \tau_1^{zy} - \hat{w}_2 \tau_2^{zy}]_{h_l}. \tag{B.10}$$

In Eqs. (B.5), (B.9) and (B.10), the components of stress tensor are given by

$$\tau_j^{xy} = \mu_j \left(\frac{\partial \hat{u}_j}{\partial y} + \frac{\partial \hat{v}_j}{\partial x}\right), \quad \tau_j^{zy} = \mu_j \left(\frac{\partial \hat{w}_j}{\partial y} + \frac{\partial \hat{v}_j}{\partial z}\right), \quad \text{and}$$

$$\tau_j^{yy} = -\hat{p}_j + 2\mu_j \frac{\partial \hat{v}_j}{\partial y}. \tag{B.11}$$

Here, $\hat{p}_j$ denote the pressure perturbations.

References

S. Ahmadi, A. Roccon, F. Zonta, and A. Soldati. Turbulent drag reduction in channel flow with viscosity stratified fluids. *Computers & Fluids*, https://doi.org/10.1016/j.compfluid.2016.11.007.

I. Barmak, A. Gelfgat, H. Vitoshkin, A. Ullmann, and N. Brauner. Stability of stratified two-phase flows in horizontal channels. *Physics of Fluids*, 28: 044101, 2016.

I. Barmak, A. Y. Gelfgat, A. Ullmann, and N. Brauner. On the squire's transformation for stratified two-phase flows in inclined channels. *International Journal of Multiphase Flow*, 88:142–151, 2017.

G. S. Beavers and D. D. Joseph. Boundary conditions at a naturally permeable wall. *Journal of Fluid Mechanics*, 30:197–207, 1967.

T. D. Blake. Slip between a liquid and a solid: DM Tolstoi's (1952) theory reconsidered. *Colloids and Surfaces*, 47:135–145, 1990.

P. Boomkamp and R. Miesen. Classification of instabilities in parallel two-phase flow. *International Journal of Multiphase Flow*, 22:67–88, 1996.

R. J. Briggs. *Electron-stream interaction with plasmas*. MIT Press, Cambridge, 1964.

C. Canuto, M. Y. Hussaini, A. M. Quarteroni, and A. Thomas Jr. *Spectral methods in fluid dynamics*. Springer Science & Business Media, New York, 2012.

Q. Cao, A. L. Ventresca, K. R. Sreenivas, and A. K. Prasad. Instability due to viscosity stratification downstream of a centerline injector. *The Canadian Journal of Chemical Engineering*, 81:913–922, 2003.

G. Chattopadhyay and R. Usha. On the Yih–Marangoni instability of a two-phase plane Poiseuille flow in a hydrophobic channel. *Chemical Engineering Science*, 145:214–232, 2016.

J. M. Chomaz. Global instabilities in spatially developing flows: non-normality and nonlinearity. *Annual Review of Fluid Mechanics*, 37:357–392, 2005.

N. Churaev, V. Sobolev, and A. Somov. Slippage of liquids over lyophobic solid surfaces. *Journal of Colloid and Interface Science*, 97:574–581, 1984.

P. G. Drazin and W. H. Reid. *Hydrodynamic stability*. Cambridge University Press, Cambridge, 2004.

C. Duprat, C. Ruyer-Quil, S. Kalliadasis, and F. Giorgiutti-Dauphiné. Absolute and convective instabilities of a viscous film flowing down a vertical fiber. *Physical Review Letters*, 98:244502, 2007.

E. Ellaban, J. Pascal, and S. D'Alessio. Instability of a binary liquid film flowing down a slippery heated plate. *Physics of Fluids*, 29:092105, 2017.

I. Frigaard. Super-stable parallel flows of multiple visco-plastic fluids. *Journal of Non-Newtonian Fluid Mechanics*, 100:49–75, 2001.

J. M. Gersting Jr. Hydrodynamic stability of plane porous slip flow. *The Physics of Fluids*, 17:2126–2127, 1974.

S. Ghosh, R. Usha, and K. C. Sahu. Double-diffusive two-fluid flow in a slippery channel: A linear stability analysis. *Physics of Fluids*, 26:127101, 2014a.

S. Ghosh, R. Usha, and K. C. Sahu. Linear stability analysis of miscible two-fluid flow in a channel with velocity slip at the walls. *Physics of Fluids*, 26: 014107, 2014b.

R. Govindarajan and K. C. Sahu. Instabilities in viscosity-stratified flow. *Annual Review of Fluid Mechanics*, 46:331–353, 2014.

E. J. Hinch. A note on the mechanism of the instability at the interface between two shearing fluids. *Journal of Fluid Mechanics*, 144:463–465, 1984.

P. Huerre. *Open shear flow instabilities. In: G. K. Batchelor, H. K. Moffatt, M. G. Worster eds. Perspectives in Fluid Dynamics: A Collective Introduction to Current Research.* Cambridge University Press, London, 2000.

P. Huerre and P. A. Monkewitz. Local and global instabilities in spatially developing flows. *Annual Review of Fluid Mechanics*, 22:473–537, 1990.

D. D. Joseph, R. Bai, K. Chen, and Y. Y. Renardy. Core-annular flows. *Annual Review of Fluid Mechanics*, 29:65–90, 1997.

A. Kaffel and A. Riaz. Eigenspectra and mode coalescence of temporal instability in two-phase channel flow. *Physics of Fluids*, 27:042101, 2015.

S. Kalliadasis, C. Ruyer-Quil, B. Scheid, and M. G. Velarde. *Falling liquid films*. Springer Science & Business Media, New York, 2011.

E. Lauga and C. Cossu. A note on the stability of slip channel flows. *Physics of Fluids*, 17:088106, 2005.

E. Lauga and H. A. Stone. Effective slip in pressure-driven Stokes flow. *Journal of Fluid Mechanics*, 489:55–77, 2003.

V. Mhetar and L. Archer. Slip in entangled polymer melts. 1. general features. *Macromolecules*, 31:8607–8616, 1998.

K. Migler, H. Hervet, and L. Leger. Slip transition of a polymer melt under shear stress. *Physical review letters*, 70:287–290, 1993.

T. Min and J. Kim. Effects of hydrophobic surface on stability and transition. *Physics of Fluids*, 17:108106, 2005.

A. Mohammadi and A. J. Smits. Linear stability of two-layer couette flows. *Journal of Fluid Mechanics*, 826:128–157, 2017.

L. Ó. Náraigh and P. D. M. Spelt. Instability of pressure-driven gas–liquid two-layer channel flows in two and three dimensions. *Journal of Fluid Mechanics*, 849:1–34, 2018.

L. Ó. Náraigh, P. Valluri, D. M. Scott, I. Bethune, and P. D. M. Spelt. Linear instability, nonlinear instability and ligament dynamics in three-dimensional laminar two-layer liquid-liquid flows. *Journal of Fluid Mechanics*, 750:464–506, 2014.

C. Navier. Mémoire sur les lois du mouvement des fluides. *Mémoires de l'Académie Royale des Sciences de l'Institut de France*, 6:389–440, 1823.

C. S. Nickerson and J. A. Kornfield. A "clea" geometry for suppressing wall slip. *Journal of Rheology*, 49:865–874, 2005.

D. A. Nield and A. Bejan. *Convection in porous media*. Springer, New York, 2006.

D. Picchi, I. Barmak, A. Ullmann, and N. Brauner. Stability of stratified two-phase channel flows of Newtonian/non-Newtonian shear-thinning fluids. *International Journal of Multiphase Flow*, 99:111–131, 2018.

M. Regner, M. Henningsson, J. Wiklund, K. Östergren, and C. Trägårdh. Predicting the displacement of yoghurt by water in a pipe using CFD. *Chemical Engineering Technology*, 30:844–853, 2007.

M. E. Rosti and L. Brandt. Numerical simulation of turbulent channel flow over a viscous hyper-elastic wall. *Journal of Fluid Mechanics*, 830:708–735, 2017.

E. Ruckenstein and P. Rajora. On the no-slip boundary condition of hydrodynamics. *Journal of Colloid and Interface Science*, 96:488–491, 1983.

I. M. R. Sadiq, R. Usha, and S. W. Joo. Instabilities in a liquid film flow over an inclined heated porous substrate. *Chemical Engineering Science*, 65: 4443–4459, 2010.

K. C. Sahu and O. K. Matar. Three-dimensional linear instability in pressure-driven two-layer channel flow of a Newtonian and a Herschel–Bulkley fluid. *Physics of Fluids*, 22:112103, 2010.

K. C. Sahu and O. K. Matar. Three-dimensional convective and absolute instabilities in pressure-driven two-layer channel flow. *International Journal of Multiphase Flow*, 37:987–993, 2011.

K. C. Sahu, P. Valluri, P. D. M. Spelt, and O. K. Matar. Linear instability of pressure-driven channel flow of a Newtonian and a Herschel-Bulkley fluid. *Physics of Fluids*, 19:122101, 2007.

A. Samanta, C. Ruyer-Quil, and B. Goyeau. A falling film down a slippery inclined plane. *Journal of Fluid Mechanics*, 684:353–383, 2011.

P. J. Schmid and D. S. Henningson. *Stability and transition in shear flows*. Springer Science & Business Media, New York, 2012.

V. Shankar and V. Kumaran. Stability of non-parabolic flow in a flexible tube. *Journal of Fluid Mechanics*, 395:211–236, 1999.

L. Sirovich and S. Karlsson. Turbulent drag reduction by passive mechanisms. *Nature*, 388:753–755, 1997.

H. B. Squire. On the stability for three-dimensional disturbances of viscous fluid flow between parallel walls. *Proceedings of The Royal Society of London A*, 142:621–628, 1933.

S. Taghavi. A two-layer model for buoyant displacement flows in a channel with wall slip. *Journal of Fluid Mechanics*, 852:602–640, 2018.

B. Tilley, S. Davis, and S. Bankoff. Linear stability theory of two-layer fluid flow in an inclined channel. *Physics of Fluids*, 6:3906–3922, 1994.

D. C. Tretheway and C. D. Meinhart. Apparent fluid slip at hydrophobic microchannel walls. *Physics of Fluids*, 14:L9–L12, 2002.

R. Usha and Anjalaiah. Steady solution and spatial stability of gravity-driven thin-film flow: reconstruction of an uneven slippery bottom substrate. *Acta Mechanica*, 227:1685–1709, 2016.

P. Valluri, L. Ó. Náraigh, H. Ding, and P. D. M. Spelt. Linear and nonlinear spatio-temporal instability in laminar two-layer flows. *Journal of Fluid Mechanics*, 656:458–480, 2010.

A.-L. Vayssade, C. Lee, E. Terriac, F. Monti, M. Cloitre, and P. Tabeling. Dynamical role of slip heterogeneities in confined flows. *Physical Review E*, 89:052309, 2014.

M. K. S. Verma and V. Kumaran. A multifold reduction in the transition Reynolds number, and ultra-fast mixing, in a micro-channel due to a dynamical instability induced by a soft wall. *Journal of Fluid Mechanics*, 727: 407–455, 2013.

O. I. Vinogradova. Drainage of a thin liquid film confined between hydrophobic surfaces. *Langmuir*, 11:2213–2220, 1995.

O. I. Vinogradova. Slippage of water over hydrophobic surfaces. *International Journal of Mineral Processing*, 56:31–60, 1999.

R. S. Voronov, D. V. Papavassiliou, and L. L. Lee. Review of fluid slip over superhydrophobic surfaces and its dependence on the contact angle. *Industrial & Engineering Chemistry Research*, 47:2455–2477, 2008.

K. Watanabe and H. Udagawa. Drag reduction of non-Newtonian fluids in a circular pipe with a highly water-repellent wall. *AIChE Journal*, 47:256–262, 2001.

K. Watanabe, Yanuar, and H. Mizunuma. Slip of Netwonian fluids at solid boundary. *JSME International Journal Series B Fluids and Thermal Engineering*, 41:525–529, 1998.

K. Watanabe, Y. Udagawa, and H. Udagawa. Drag reduction of Newtonian fluid in a circular pipe with a highly water-repellent wall. *Journal of Fluid Mechanics*, 381:225–238, 1999.

S. G. Yiantsios and B. G. Higgins. Linear stability of plane Poiseuille flow of two superposed fluids. *Physics of Fluids*, 31:3225–3238, 1988.

C.-S. Yih. Instability due to viscosity stratification. *Journal of Fluid Mechanics*, 27:337–352, 1967.

X.-Y. You and J.-R. Zheng. Stability of liquid-liquid stratified microchannel flow under the effects of boundary slip. *International Journal of Chemical Reactor Engineering*, 7:1–12, 2009.